



LAWRENCE
LIVERMORE
NATIONAL
LABORATORY

Sample Preparation on the Micro-Scale: Digestion, Separation and Identification

E. J. Fong

July 3, 2013

Disclaimer

This document was prepared as an account of work sponsored by an agency of the United States government. Neither the United States government nor Lawrence Livermore National Security, LLC, nor any of their employees makes any warranty, expressed or implied, or assumes any legal liability or responsibility for the accuracy, completeness, or usefulness of any information, apparatus, product, or process disclosed, or represents that its use would not infringe privately owned rights. Reference herein to any specific commercial product, process, or service by trade name, trademark, manufacturer, or otherwise does not necessarily constitute or imply its endorsement, recommendation, or favoring by the United States government or Lawrence Livermore National Security, LLC. The views and opinions of authors expressed herein do not necessarily state or reflect those of the United States government or Lawrence Livermore National Security, LLC, and shall not be used for advertising or product endorsement purposes.

This work performed under the auspices of the U.S. Department of Energy by Lawrence Livermore National Laboratory under Contract DE-AC52-07NA27344.

Dissertation Prospectus

Sample Preparation on the Micro-Scale: Digestion, Separation and Identification

Boston University
Biomedical Engineering

Erika Fong
(925) 423-3596
ejfong@bu.edu

Date of Defense: July 18th 2013
Location of Defense: Room 705, 44 Cummington St., Boston, MA

Thesis Advisor & Committee Chair: Muhammad H. Zaman, PhD

Committee Members:

Mario Cabodi, PhD

Ahmad Khalil, PhD

Maxim Shusteff, MS

Bela Suki, PhD

Muhammad H. Zaman, PhD

Contents

Project Summary.....	1
Background and Significance	2
Aim 1: Sample Digestion for Microfluidics	2
Sputum	2
Existing Devices	2
Sputum Rheology: Particle Tracking Microrheology	3
Aim 2: Sample Purification -Acoustofluidics	4
Background	4
Existing Devices	5
Aim 3: Physical Cell Biomarkers.....	6
Impedance Spectroscopy.....	7
Single Cell Rheology in Microfluidics	8
Capture Arrays	10
Existing Work	10
Dengue Virus	11
Aim 1: Applying Particle Tracking Microrheology to Sputum	11
Research Design.....	12
Simulations	12
Experimental Studies	13
Preliminary Results.....	14
Simulations	14
Experimental Studies	15
Aim 2: Acoustofluidic Separation.....	16
Research Design.....	16
Device Design.....	17
Calibration.....	18
Cell-Virus Separations	18
Virus Infection Monitoring	19
Preliminary Results.....	19
Focusing Through the Wall.....	19
Device Optimization	20
Cell-Virus Separations	21
Virus Infection Monitoring: Potential challenges and strategies	21

Aim 3: Single Cell Impedance and Mechanics.....	22
Research Design.....	22
Potential Challenges and Strategies	23
Expected Results.....	24
Conclusion	24
Acknowledgements.....	24
References.....	25
Timeline	31
Author’s Vitae.....	32

Project Summary

Microfluidics has promised to revolutionize bio-analytical techniques with the creation of Lab-On-a-Chip (LOC) devices that reduce the reagents, complexity, time and infrastructure required to perform laboratory procedures and by enabling novel measurements.¹⁻⁶ However, the issue of sample preparation remains a major challenge for many of these devices.^{7,8} Firstly, achieving uniform sample processing is essential when operating on the micro-scale.⁸ In microfluidic devices, often only microliters of sample are required for each test; therefore the sample must be homogenized before a portion is taken for analysis in order to ensure dependable results. Understanding the rheology of the sample on the micro-scale is important in optimizing devices and understanding how to process samples.

Many traditional techniques require samples to be diluted in large volumes of reagents, and then particles of interest must be purified and concentrated.^{8,9} Most methods used to selectively extract particles are based on size.¹⁰ This approach is beneficial because it can be generally applied to most biological samples since different types of specimen have drastically different length scales. For example, mammalian cells are tens of micrometers, while bacteria are only a few micrometers, and viruses are tens to hundreds of nanometers in diameter.

While many exceptional devices have been designed to extract specific biological specimen based on size differences, expanding the parameters used to identify and select for specific particles would be highly advantageous. Cell staining is ubiquitous to identify and study cells, however, intercellular staining is often required which requires cell permeabilization and causes cell death. Antibody markers, such as expressed surface proteins, are highly specific, but in some cases can be too limiting. For example, identifying circulating tumor cells by epithelial surface markers may lead some cells with metastatic potential to be overlooked.¹¹ Physical markers promise to offer an alternative to chemical markers for cell identification and analysis. Therefore, I seek to study an array of physical characteristics to identify specific cells. Cell impedance will be investigated, since impedance spectroscopy enables the cell interior to be probed.¹² In addition, cell deformation will be measured which has been correlated with a number of cell states.^{13,14} The proposed platform will also allow optical measurements to be made.

Based on the current limitations in sample preparation, I aim to address three key issues in biological sample preparation. They are: the rheology of viscous samples, selective extraction and washing of cells utilizing size differences, and determining relevant cell properties for cell analysis.

First, a method to passively measure the microstructure of biological samples is explored. I examined changes in human sputum with degradation agents and investigated sputum heterogeneity on the micro-scale. Next, acoustic forces are used to wash cells and investigate novel applications in studying viral cell dynamics for this technology. Lastly, rheology and cell manipulation will be combined on chip to investigate cell physical properties. Studying sputum highlights the vast differences in biological specimen. The acoustic device both underscores how general cell properties can be used to preferentially separate cells from other contaminants, and the limited properties used to manipulate cells. Therefore, to interrogate cell properties, single cells will be probed with a variety of methods to get relevant data despite highly heterogeneous populations. These studies will enhance existing attempts to discriminate cell populations and cell states, by allowing multiple physical properties to be correlated with cell condition.

Specific Aim 1: Develop and optimize a quantitative method to measure heterogeneous complex biological samples.

Specific Aim 2: Characterize an acoustic separation platform to move cells from a sample stream to a clean buffer stream. (2a) Quantify the effect of wall thickness on acoustic focusing and optimize device

operation. (2b) Wash human lymphocytes spiked with Dengue virus (DENV). Use device to monitor DENV infection.

Specific Aim 3: Investigate cell impedance in relation to mechanical and optical form and function. (3a) Engineer an electrode design that enables dielectrophoretic manipulation, electrodeformation and impedance spectroscopy. (3b) Use this device to investigate changes in cell properties upon infection with DENV.

Background and Significance

Many exciting microfluidic devices have been and are being developed to enrich and advance bio-analytical techniques, however, challenges in performing sample preparation steps limits the adoption and significance of these devices.⁷ Few commercially available devices use microfluidics, one of the limited commercial devices, Cephid's GeneXpert uses a macroscopic sample preparation approach.¹⁵ While numerous advances have been made in enabling sample preparation steps to be performed on chip,^{9,16} many devices have not been tested with complex biological samples, especially those intended to measure specific cell properties.^{4,5,17,18} One of the ultimate goals in biomedical research is to be able to take a complex clinical samples, of any type, and analyze and experiment with this sample to get results. Ideally, the sample can be studied in its native state to take full advantage of using real clinical samples. Therefore, it is necessary to perform all procedures with minimal disruption and changes to the sample. Thus, label-free noninvasive methods are preferred. With the mindset of developing tools for research, I aim to address three major challenges in sample analysis using label-free, non-invasive techniques. This work will investigate sample properties, the purification of cells from samples, and label free methods to analyze cells. Taken together, the work accomplished in this thesis will add to the toolset available to study samples noninvasively, thus bringing us one step closer to the ultimate goal of analyzing clinical samples in their native state.

Aim 1: Sample Digestion for Microfluidics

Micro-devices offer the advantages of a reduced footprint, minimal sample and reagent consumption, consistency across different operators and speed. However, samples must meet certain criteria before being introduced to these devices. Challenges with clogging and inadequate mixing in micro-devices generally require sample preparation to be performed off chip. Additionally, when only small volumes of sample are required⁶ it is necessary to make sure the tested portion is representative of the entire sample. Since sputum is a key biological material for diagnosis and notoriously difficult to work with,^{8,19} it will be the focus of this study.

Sputum

Sputum is expelled when a patient coughs and is essential as a diagnostic specimen for lower respiratory tract infections. Sputum is used for a variety of tests including staining, culture, and PCR. While the modes of pathogen detection may be drastically different, it is usually necessary to process the sputum prior to applying a diagnostic test. Chemicals such as sodium hydroxide (NaOH), and N-acetyl-L-cysteine (NALC) can be added to sputum to digest the complex matrix of mucins, heavily glycosylated proteins. Depending on the assay, oftentimes additional mechanical methods are used such as vortexing the sample.

Existing Devices

Ideally, all sample preparation steps would be performed within the microfluidic device. However, few devices can accommodate highly viscous, elastic samples such as sputum. E. coli at concentrations as low as 33 colony forming units/ml were detected in mucin (stimulating sputum) using a microfluidic origami style device.²⁰ This device is drastically different than traditional microfluidic devices, and does not employ micro-channels, but uses capillary action between layers of absorbent

materials to digest the sample, lyse cells and extract nucleic acid (Figure 1). While the trend towards using paper microfluidics is ideal for point-of-care (POC) devices, it is impossible to use many of the sophisticated technologies developed for traditional microfluidic devices.

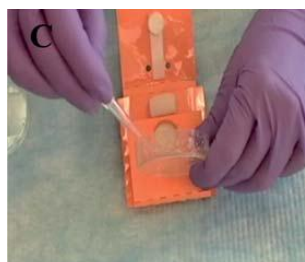


Figure 1 Operator placing mucin on DNA extraction microfluidic origami device. Taken from [20].

Cepheid recently released a contained polymerase chain reaction (PCR) platform that uses disposable microfluidic cartridges to test sputum for tuberculosis (TB) bacilli.²¹ Samples are combined with chemical reagents and mixed before they can be pipetted into the cartridge and placed in their custom PCR machine. While this system is revolutionary for TB diagnosis, especially due to the ability to detect drug resistance, it is unlikely to be deployed in smaller rural health clinics. This system requires a stable power source, calibration and maintenance. In regions where TB is endemic there is a need for a TB diagnosis device that can be deployed with even less resources.²² Investigators at Harvard are exploring methods to adapt their on-chip nuclear magnetic resonance (NMR) device to TB diagnosis (Figure 2).²³

Magnetic particles coated with antibodies bind to bacilli and cause them to cluster together, which results in a decrease in relaxation time that is detected via NMR. Theoretically this method can measure turbid samples; however, some degree of sample processing will be necessary for samples to flow through the micro-channels.

Each device has very different requirements for sample quality. In order to optimize sample preparation the physical structure and make up of sputum before and after liquefaction is of particular interest. A common procedure for digesting sputum for culture and acid fast smears is to liquefy samples by diluting in an equal volume of 2-4% NaOH and 1% NALC, and then further dilute in physiological buffer (PBS).²⁴⁻²⁸ This method results in large volumes of sample, however many microfluidic devices require only small volumes of samples,²⁹ and large sample volumes must be concentrated to permit sensitive measurements to be made.^{9,30} I have investigated a method to observe the degradation of sputum on the micro-scale upon the addition of small volumes of highly concentrated NaOH.

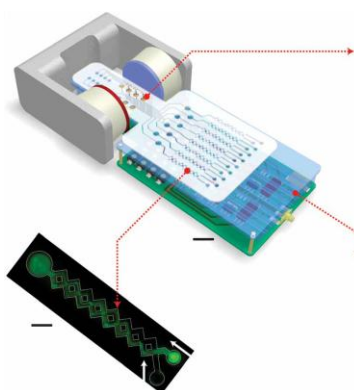


Figure 2 Schematic of on-chip NMR device. Taken from [23]

Sputum Rheology: Particle Tracking Microrheology

Traditional rheometers measure bulk sample properties and often destroy the sample in the process. To understand the properties of sputum on length scales relevant to microfluidic devices it is necessary to probe sputum microrheology.

Over the last decade, Particle Tracking Microrheology (PTM) has emerged as a valuable tool to get precise measurements of localized viscoelastic properties of complex fluids, ranging from colloids to *in vivo* biological samples.³¹⁻³⁴ Instead of mechanically shearing the sample at different rates, the thermal motion of sub-micron sized particles embedded in the sample is measured optically to passively probe the microstructure of complex fluids. By looking at the mean squared displacement (MSD) at different intervals it is possible to measure a sample's viscoelastic behavior. PTM has been used in a wide array of applications from the assessment of cell stiffness to probing the diffusive properties of therapeutic agents in mucus and has the potential to elucidate the behavior and function of heterogeneous and inherently complex biological fluids including sputum.^{19,35-40}

Samples are required to be at complete motion equilibrium before beginning measurements, which limits the capacity of this technique to measure dynamic processes.^{37,38,41,42} A variety of methods have been developed to decouple superfluous motion from thermal motion, however these methods

mostly focus on eliminating stage drift or vibrations of the entire sample and cannot address directed movement within specific portions of the sample.^{38,43,44} Dynamic processes, such as adding digestion agents to sputum, often create local currents causing beads to move in a directed manner. Beads in less viscous environments will be more affected and results will not be consistent. To make this exceptional technique accessible, methods to apply PTM to heterogeneous dynamic systems will be investigated.

Aim 2: Sample Purification -Acoustofluidics

Once the sample is digested and can flow through a microfluidic chip it is possible to perform many sample preparation procedures on chip.⁴⁶⁻⁴⁸ A common procedure is to exchange the suspending media around cells. Acoustophoresis is well established as a method to manipulate biological species, and does not affect cell expression or viability.⁴⁹ Despite the popularity of acoustophoresis for size based separation it is seldom applied to cell-virus mixtures.⁵⁰ In this aim acoustic forces will be used to separate cells and viruses.

Background

When an acoustic standing wave propagates through media it generates a primary radiation force. The primary force can be described as:

$$F = -\left(\frac{\pi p_0^2 V_p \beta_w}{2\lambda}\right) \cdot \phi(\beta, \rho) \cdot \sin(2kx) \quad \text{Equation 1a}$$

$$\phi(\beta, \rho) = \frac{5\rho_p - 2\rho_m}{2\rho_p + \rho_m} - \beta_p / \beta_m \quad \text{Equation 1b}$$

Where ϕ is the contrast factor, p_0 is the pressure amplitude, V_p is the particle volume, β is the compressibility, k is the wave number, ρ is the density, λ is the wavelength, and x is the distance from the pressure node. Subscripts p and m stand for the particle and the medium respectively. The primary force acts to focus particles to either the pressure nodes or anti nodes depending on the sign of the contrast factor. Solid particles like cells are generally focused towards pressure nodes while particles like lipids are focused to pressure antinodes in water. The acoustic force is highly sensitive to size differences since it scales with volume, making it attractive as a size based separation technique.

Due to the simplicity of device design, fabrication and operation, Lund type acoustic microfluidic devices are popular for particle manipulation. Channels are fabricated in materials that enable acoustic waves to be transmitted with little losses. When a piezoelectric coupled to the device is excited at the appropriate frequency standing waves are created within the channel (Figure 3). The pressure amplitude in Equation 1a is directly related to the voltage supplied to the piezoelectric. Generally, the channel width is a half wavelength to create a single node in the center and two antinodes at the channel walls. However, this design is fundamentally limited for particle separation and concentration. For optimal concentration, a trifurcation is required at the outlet^{45,48,51} which adds complexity and may alter the laminar profile reducing separation efficiency. Additionally, focusing particles to the walls may increase wall adsorption, leading to a lower recovery of particles.

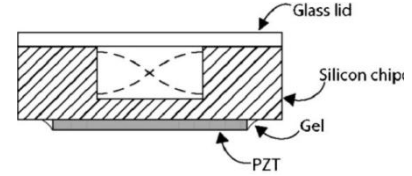


Figure 3 Schematic of Lund type acoustic micro-channel operating in the half wavelength mode. Taken from [45].

Existing Devices

Acoustic Devices Generally, acoustic separation devices rely on either migration velocities of different sized particles or on differences in contrast factors. Using differences in contrast factors to separate particles is attractive since this process is definitive and not as time sensitive. However, the majority of biologically relevant particles, such as cells, have similar contrast factors. While this technique has been used successfully to separate lipids from blood,⁵⁴ it is often difficult to separate biological particles without using specific buffers. Petersson et al. adjust the fluid density to separate platelets and red blood cells with 92% of red blood cells (RBC) exiting in one outlet and 99% of platelets exiting in another outlet (Figure 4).⁵² Improvements to this design include pre-focusing in both the horizontal and vertical direction. First all species are focused in two dimensions to the channel edges and midline. The sample then enters the next region where another transducer induces a node at the center of the channel. This design requires two focusing regions and thus two transducers excited at different frequencies (Figure 5). Using this design, white blood cells spiked with circulating tumor cells, were separated with 79-99% efficiency.⁵³ Existing work also suggests that acoustic separation can be used to distinguish viable and non-viable cells, as cells that have undergone apoptosis are smaller.⁵⁵

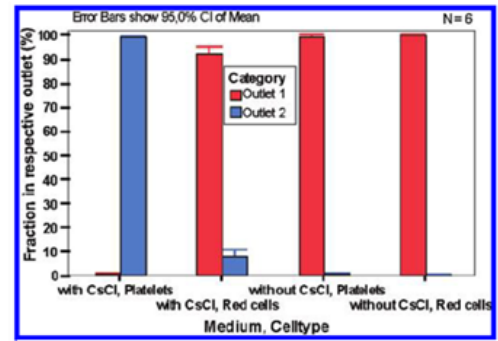


Figure 4 Separation of RBCs and platelets using a cesium chloride to alter medium density. Taken from [52].

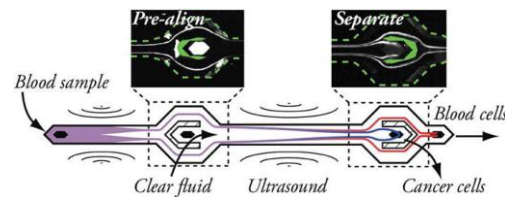


Figure 5 Schematic of pre-focusing for acoustic separation of cancer cells in blood. Taken from [53]

Cell-Virus Separation Very few microfluidic methods exist to separate cells and viruses. However, a number of devices move cells across fluid interfaces.^{46,56} Theoretically, these devices should be able to separate cells and viruses as viruses should remain in the original solution due to the drastic size difference. Most microfluidic devices that address virus isolation are interested in pathogen detection and extract viral nucleic acid from samples after lysing cells and other constituents, rather than extracting live viruses and cells.¹⁶ Devices that have been used to separate viable cells and viruses do not achieve high separation efficiency or throughputs. Zhao et al. layer blood over a buffer stream and use cell sedimentation to isolate cells from spiked viruses.⁵⁷ This method is inherently slow since separation depends on residence time. The device was operated at 6 μ L/min.⁵⁷ Colleagues at Lawrence Livermore National Laboratory (LLNL) previously designed an acoustic cell-virus separation device; however, complete separation was not possible. A cell-virus sample and buffer solution were injected in parallel using a H-filter design, and was acoustically excited such that cells focused to the center of the channel, while viruses remained in the lower half (Figure 6).⁵⁰ Since the cells did not cross the fluid interface between the sample input and the buffer stream, cells could only be enriched from viruses, not separated. Generally cell and virus separation is achieved via centrifugation.⁵⁸ While well established, this method is a fairly time intensive benchtop technique. In addition, centrifugation has been shown to increase infectivity for certain viruses, and may change cell-virus

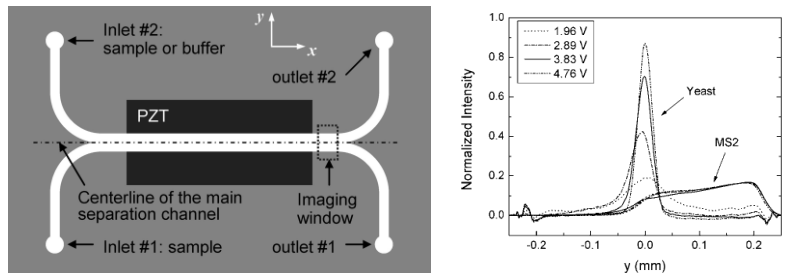


Figure 6 Acoustic cell-virus enrichment device previously designed at LLNL. Left: Schematic of H-filter design. Right: intensity profile of cell and virus distribution across channel width. Taken from [50].

While well established, this method is a fairly time intensive benchtop technique. In addition, centrifugation has been shown to increase infectivity for certain viruses, and may change cell-virus

interaction dynamics.^{59,60} While centrifugation is useful to accelerate diagnosis,⁵⁸ it may confound experiments trying to study cell-virus interactions. Therefore an alternative method to extract viable cell and viruses from samples is desired.

Drawing upon concepts that have been previously demonstrated, including the H-filter,⁶¹ asymmetric node position,⁶² and acoustically transparent membranes,⁶³ a unique acoustic focusing technique to enable high efficiency extraction of cells will be presented. The ability to arbitrarily place the acoustic pressure node by subdividing channels will be investigated. Arbitrary node placement can reduce the complexity of device fluidics, reduce species absorbed to the wall, and enable more efficient particle separation.

Aim 3: Physical Cell Biomarkers

Correlate cell impedance, deformability, size and optical properties with cell state and function.

While size based separation techniques, like acoustophoresis, are able to discriminate between some cell types, it cannot be used perform more sensitive separations of similarly sized cells. The majority of methods for cell separation and identification using physical properties are dependent on differences in cell size.¹⁰ Therefore, for precise identification of cells, highly specific proteins are usually stained for. Cells can be identified by histology or by fluorescence activated cell sorting (FACS). Histology is an inherently slow process that requires highly skilled personnel to interpret results. FACS can screen populations of 10^4 - 10^6 cells, however, nearly all assays require fixing and staining.⁶⁴ Any assay that requires cell staining is cumbersome due to incubation and wash steps that change the cell properties, and makes **time-resolved analysis impossible**. To stain intracellular components usually the cell membrane must be irreversibly permeabilized, which kills the cell. Binding assays can also be used to select for specific cells based on surface markers. While these techniques have been effective to isolate specific cells,^{65,66} they will miss cells that do not express these markers. For example, a widely accepted limitation of CellSearch, an FDA approved CTC test, is that metastatic cells that do not express the targeted surface marker, epCAM, will be overlooked.^{11,67} Both these techniques suffer limitations inherent to chemical biomarkers. They both alter the cells, either by introducing a dye or coupling them to beads or surfaces, making downstream analysis difficult if not impossible. Furthermore, multiple measurements cannot be performed on the same cell at different time points. Chemical markers are so specific they are at risk to miss cells that have adapted to use other proteins. Therefore physical biomarkers will be investigated to distinguish cell state.

Despite the success of cell cytometers that measure physical cell properties, such as impedance⁶⁸⁻⁷² and deformability,^{2,73} these cytometers have not gained widespread use. Given the potential for impedance measurements to be integrated into cytometers, and the ability to probe different cell properties, cell impedance is grossly underused as a parameter to characterize cells. While existing studies have shown that different cell lines have different impedance spectra,⁷⁴⁻⁷⁶ and changes in cell state can be monitored,^{68,77,78} correlating impedance to other physical and chemical biomarkers promises to make impedance spectroscopy more accessible.

My vision is to engineer a cell culture platform that enables single cell size, impedance, deformability and optical properties to be measured over time. In this thesis, a single cell measurement site will be designed that can be scaled to a large array. This work will immediately address the limited techniques available to study cell structure and function in a noninvasive, time resolved manner, and set the stage for the discovery of novel biomarkers as multiple modes of measurement are incorporated down the line.

Impedance Spectroscopy

Impedance spectroscopy is ideal for microfluidics and for integration into flow cytometry. Microfabrication techniques pioneered and refined by the microelectromechanical systems (MEMS) community give us high control and flexibility over electrode design and enable sophisticated electrical procedures to be performed on chip.

For single cell impedance spectroscopy, the resistance of cells is measured between two electrodes. Depending on the frequency used different parts of the system can be probed. At intermediate frequencies (1-100MHz) the cell membrane will act as an insulator and impedance will be related to cell size. At high frequencies (>100MHz) the cell membrane capacitance is short circuited, and it is possible to probe the cell interior (Figure 7).¹² Although cell size has been observed to affect impedance throughout the range of frequencies, it is possible to normalize by size and cell position by measuring impedance at a low and high frequency.^{68,79}

For flow through impedance spectrometers differential impedance spectroscopy is often employed where cells pass through two sets of electrodes. This makes measurements less susceptible to drift, reduces noise of the system, gives information about cell velocity, and is ideal for flow cytometry.¹² Cheung et al. use this set up to measure a shift in impedance spectra in red blood cells with fixation (Figure 8).⁶⁸ However, the resolution is limited due to current leakage.¹⁸ Ideally, the electric field should be as uniform as possible to limit the effects of cell location on measurements. To achieve a uniform electric field, electrodes should be similar in size to the target cells and placed on the sides of channels. However, fabricating electrodes in one plane is much easier to achieve and has been used to perform impedance spectroscopy.⁸⁰

Other devices use only two electrodes to measure impedance spectra. Best results are achieved when there is good electrical contact between the cell and the electrodes.⁸¹ Usually cells are trapped in physical traps,^{74,75,82} which can limit current leakage and allow cell membrane capacitance and cytoplasm resistivity to be probed.¹⁸

Optical microscopy is the primary mode of studying cells, even though it is invasive, slow and labor intensive. In contrast, impedance spectroscopy has been extensively studied to measure cell properties, and can be performed quickly, is fairly noninvasive and does not require cell staining. This work aims to identify specific frequencies where impedance spectra is correlated with cell state, and set the stage for a platform that enables multiple cell properties to be measured over time.

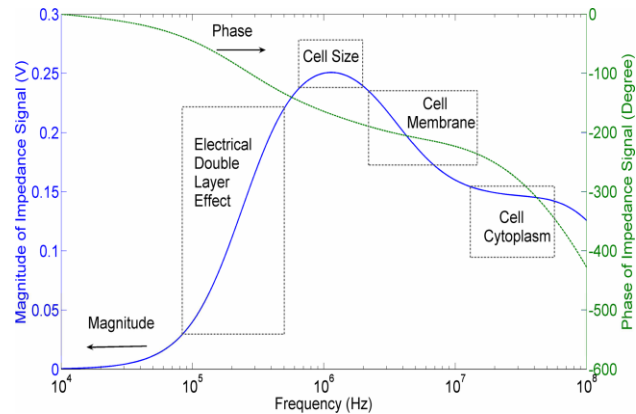


Figure 7 Simulated impedance spectra of a cell measured in differential mode. Taken from [12].

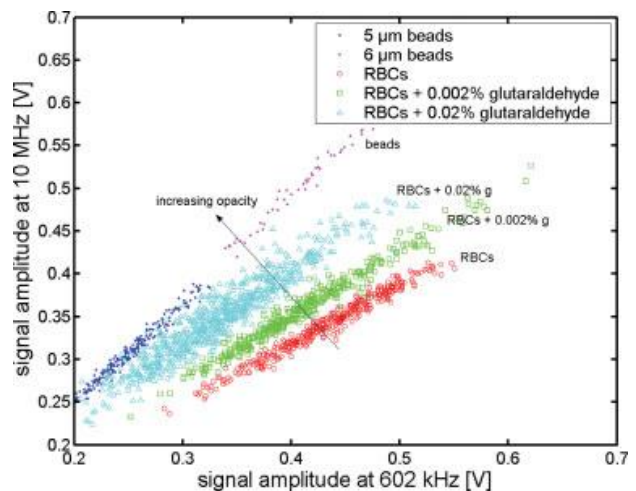


Figure 8 Impedance spectra at two different frequencies for RBC with varying degrees of fixation. Taken from [68].

Single Cell Rheology in Microfluidics

Micropipette Aspiration To measure cell stiffness or deformability there are a number of methods used. Micropipette aspiration is regularly used to measure cell viscoelasticity.⁸⁴ This method is sensitive to cell membrane properties and cell orientation and forces range from pN to nN.^{84,85} This method is easily amendable to a microfluidic platform, and measurements of human neutrophil cortical tension made via microfluidic micropipette aspiration are within the range reported using traditional micropipette aspiration.⁸³ Using this technique, human lymphocytes, neutrophils, bladder cancer cells, and mouse lymphocytes are measured and shown to have different rigidity (Figure 9).⁸³ Similarly, by measuring transit time, or required pressure for a cell to traverse a constriction it is possible to obtain a measure of cell deformability fairly easily in a microfluidic device.^{73,82} Chen et al. measure transit time through a long narrow constriction channel and cell impedance at 100kHz.⁸² Using a neural network they are able to successfully classify osteoblasts and osteocytes 97.3% of the time (Figure 10).⁸²

Hydrodynamic Stretching Gossett et al. use hydrodynamic stretching to study cell deformability in clinical pleural effusion samples.² Their device measures cells in an ultra-high throughput manner, measuring up to 2000 cells/second with forces in the μN range. Using this technique they can predict clinical outcomes with up to 91% sensitivity and 86% specificity.² However, it is difficult to perform any additional measurements in conjunction with deformability using this set up since cells are moving at such high speeds. A specialized high speed camera is required to image cells.

Optical Trapping Double beam optical traps (termed optical stretchers) have also been used to measure cell deformability in a flow through manner at rates up to 1 cell/minute, and generate forces in the 100s of pN range.^{1,86} Using this method breast cancer cell populations with varying degrees of malignancy are shown to have different deformability (Figure 11).⁸⁶ This method requires aligned lasers to generate stretching forces along the laser axis.

Electrodeformation Another method to measure cell deformability is by exposing the cell to a non-uniform electric field. The field causes dipole moments to form within the cell and the cell moves along the electric field gradient. Force for a uniform sphere placed in a sinusoidal electric field is proportional to the square of the gradient of the electric field (Equation 2a). The force will be directed towards the region of high electric field density (positive dielectrophoresis) if $K(\omega)$, the Clausius-Mossotti factor is positive,

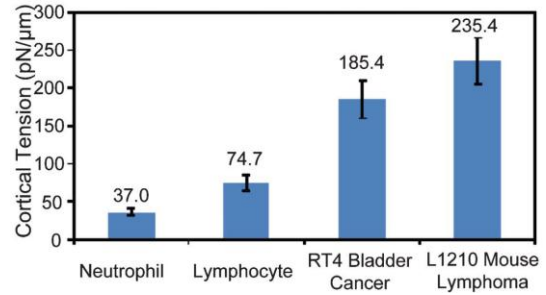


Figure 9 Cortical tension as a measure of rigidity measured via microfluidic micropipette aspiration. Taken from [83].

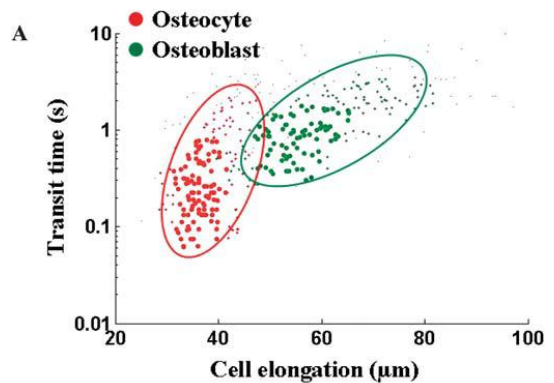


Figure 10 Different cell types can be distinguished by transit time and cell elongation through a narrow constriction channel. Taken from [82].

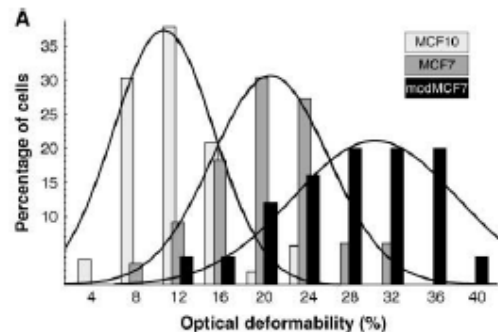


Figure 11 Deformability of breast cell lines of varying malignancy as measured by an optical trap. Increased metastatic potential is correlated with increased deformability. Taken from [86].

The force will be directed towards the region of high electric field density (positive dielectrophoresis) if $K(\omega)$, the Clausius-Mossotti factor is positive,

and towards the region of low field density if it is negative (negative dielectrophoresis). This depends on the particle and medium permittivity, ϵ , and conductivity, σ , denoted by subscripts p and m respectively (Equation 2b and 2c). ω is the frequency of the electric field.

$$\langle F_{dep}(r) \rangle = \pi \epsilon_m R^3 \text{Re}[K(\omega)] \cdot \nabla |E(r)|^2 \quad \text{Equation 2a}$$

$$K(\omega) = \left(\frac{\epsilon_p - \epsilon_m}{\epsilon_p + 2\epsilon_m} \right) \quad \text{Equation 2b}$$

$$\epsilon = \epsilon + \sigma / (j\omega) \quad \text{Equation 2c}$$

This method, dielectrophoresis, is commonly used to manipulate mammalian and bacteria cells.⁸⁹ If the field power is further increased cells are stretched via electrodeformation (Figure 12). This deformation can be observed with an optical microscope and cell properties can be calculated. Electrodeformation is fairly easy to accomplish in comparison to other techniques, and is readily amendable to microfluidic devices. In theory the only requirement is an inhomogeneous electric field, which can be produced by using electrodes of different sizes. Cells experience a much stronger dielectrophoretic force if they experience positive dielectrophoresis and move towards the region of high electric field. Positive dielectrophoresis is achieved by using low conductivity media. Forces are on the order of 10s of nN.⁹⁰

Cells are deformed by the electric field and image analysis is performed to determine rheological properties. Analysis as simple as looking at the elongation show that red blood cells from patients with spherocytosis are less deformable than normal red blood cells.⁹¹ Using a numerical model Chen et al. were able to measure Young's modulus of cervical cancer cells within the range measured in conventional micropipette aspiration.⁸⁷ Using a numerical model they simulate deformation expected for materials with different Young's modulus and compare to observed deformation to get a quantitative measure of cell stiffness to compare to other methods. MacQueen et al. use electrodeformation to show Chinese hamster ovary and promonocytes have distinct strain and relaxation profiles (Figure 13).⁸⁸

Cell rheology is a key parameter in cell function^{13,92} and these results suggest that it is possible to identify cells based on their stiffness or deformability in a microfluidic setting.

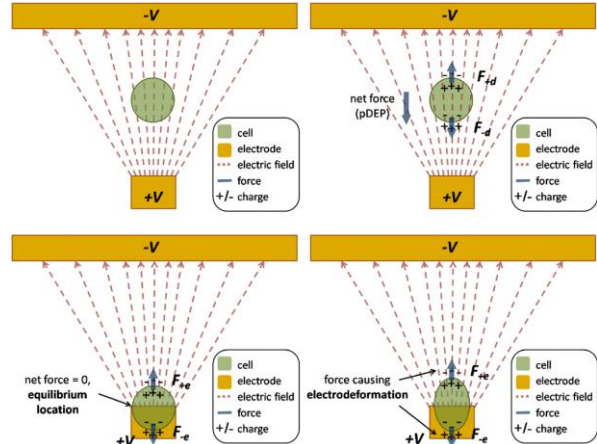


Figure 12 Schematic of positive electrophoresis and electrodeformation. From top left to bottom right: (i) The cell is exposed to a non-uniform electric field, which polarizes the cell, forming induced dipoles (ii). The cell then migrates to the equilibrium position (iii). The electric field intensity is increased and cells experience electrodeformation (iv). Taken from [87].

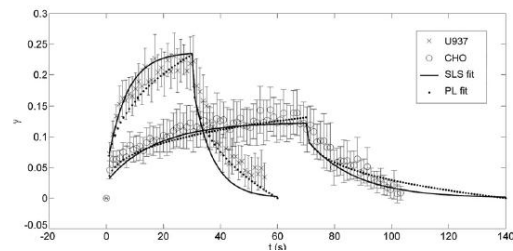


Figure 13 Strain and relaxation data for CHO and U937 cells measured via electrodeformation. Data was fit to a standard linear solid (SLS) and a power law (PL) model. Taken from [88].

Capture Arrays

Cell capture arrays are an alternative to cytometry to study cell populations and obtain statistically relevant single cell data. In addition, it is possible to make measurements at multiple time points on the same cells. Hydrodynamic cell arrays use physical structures that are loaded with one or more cells (Figure 14).⁹³ Experiments investigating enzyme kinetics,⁹³ electrodeformation⁹¹, and cell staining⁹⁴ utilizing automated image analysis have been performed on cells positioned in these arrays. Electric trap arrays utilizing dielectrophoresis to confine cells are also possible.⁹⁵

Existing Work

Chen et al. measure cell impedance and transit time through a narrow constriction to classify wild type murine breast cancer cells and drug resistant cells.⁸² These two cell types are similar in size and it is unlikely they could be distinguished by size alone. By measuring both impedance amplitude ratio and transit time they are able to successfully classify the two cell types 70.2% of the time, while using one parameter alone gave success rates of only 57.5 and 59.6%, respectively.⁸⁷ Subsequent work measured cell impedance at multiple frequencies to deduce cell cytoplasm resistivity and membrane capacitance.¹⁸ However, cells must be measured serially and their device design is not scalable to measure many cells in parallel. Moreover, this method is fairly invasive, as cells must squeeze through a narrow constriction region. Their work underscores the importance of measuring multiple properties of cells to get a full picture. This work aims to make similar measurements using less invasive techniques in a way that can be scaled to measure multiple cells over time.

Malleo et al. use a hydrodynamic capture array to measure cell lysis and poration upon addition of chemical fixation reagents and toxins via impedance changes.⁷⁸ Incorporating additional modes of measurements will significantly advance this technology, and will require a completely different device to be designed. This work seeks to correlate impedance measurements with the physical structure of cells by investigating optical and mechanical properties in addition to the impedance spectra.

There is a severe deficit in noninvasive biomarkers – that is, cell properties that can be measured without major effects on cell viability or metabolic activity. Numerous studies have correlated virus infection with changes in cell monolayer impedance which can be measured with little damage to the cells.⁹⁶⁻¹⁰⁰ However, investigations on the single cell level are limited.^{101,102} This work aims to expand the available range of noninvasive biomarkers by identifying cell electrical characteristics that predict changes in cell physical parameters, disease state, or biological activity. Methods to monitor cells over time are severely limited, especially at the single cell scale. Monitoring changes taking place in single cells will lead to a fuller characterization of “normal” cell parameters, to which disease states can be compared. To address these issues, in aim 3 multiple interrogation modalities will be integrated: mechanical, electrical and optical. Measuring many properties at the same time will create a truly general-use capability, applicable to studying cells in a host of different applications. The goal of this work is to lay the foundation for a device that enables single cells to be monitored over time. Identifying new label-free biomarkers will allow investigators to detect and separate cells of interest without significantly altering them, enabling novel assays to be developed, and exciting downstream analyses to be performed.

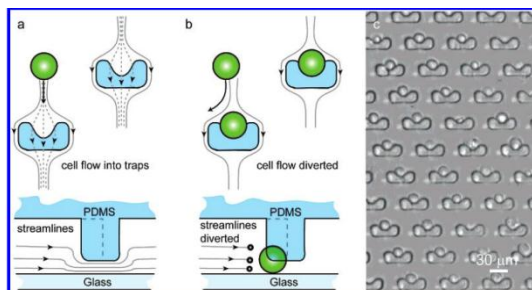


Figure 14 Single cell hydrodynamic capture array. Taken from [93].

Dengue Virus

DENV causes 50-100 million infections per year¹⁰³ and can lead to hemorrhagic fever, and toxic shock syndrome which often result in death. Currently there are no vaccines available or specific drugs to treat DENV infection, and nearly 3.6 billion people live countries where DENV is endemic.¹⁰⁴ DENV is categorized as a category A priority pathogen by the National Institute of Allergy and Infectious Diseases (NIAID), indicating that it is among the pathogens which pose the highest risk to national security and public health.¹⁰⁵ Category A priority pathogens can be easily disseminated or transmitted from person to person, and have high mortality rates. To generate effective therapies and prevention strategies it is necessary to understand the intricate nature of DENV infection and how it leads to severe disease. Despite the extensive research into this virus, many questions remain. Such as, why does prior infection with one strain often result in more severe infection when infected with a different strain of the virus?¹⁰⁶ Therefore, it is imperative to develop tools to help enable basic science research of virus infection.

Cell culture is a valuable platform that gives investigators experimental flexibility and high control over the environment to probe specific hypotheses. While a culture plate is far from an *in vivo* system, the accessibility, flexibility, control and cost effectiveness make cell culture a mainstay of many laboratories. Centrifugation is required for nearly all laboratory techniques, especially when working with cell culture. However, spinoculation has been used to enhance some viruses infectivity, such as cytomegalovirus, herpes simplex virus, blue-tongue virus, retroviruses and HIV-1.¹⁰⁷ This technique involves centrifuging cells and virus together. Usually cells are cultured as a monolayer and virus is placed on the monolayer and spun down. Centrifuging hepatitis C virus with liver cells for a short as 30 minutes at 1000 x g significantly increases the amount of viral RNA extracted compared to non-centrifuged controls.¹⁰⁸ In this study, the increase in recovered viral RNA is directly related to the time, and the speed of centrifugation.¹⁰⁸ As hepatitis C and DENV are both in the virus family *Flaviviridae*, these results suggest that centrifugation may affect DENV infection dynamics. While traditional centrifugation protocols usually involve centrifuging cells in suspension at high rates for shorter times than spinoculation protocols, extrapolating these results suggests that even at short time scales centrifugation can significantly change virus infection dynamics if the centrifugal forces are high enough. An alternative method to centrifugation is desired. Therefore, in aim 2 I will focus on developing an acoustic cell virus separation platform and use it to assess the effect of centrifugation on DENV virus infectivity.

Monitoring cell infection with viruses is essential for understanding infection dynamics, and for vaccine and drug development. However, relatively few methods exist to monitor cellular changes upon infection with virus. Cytopathic effects are observable via microscopy for some viruses and provide mostly qualitative measurements of cell health. Traditional methods to measure viral replication in cell culture include plaque assays and hemagglutination assays. Plaque assays require serial dilution of culture supernatant onto healthy cultured cells to determine viral titer. Hemagglutination assays assess the active viral particles by observing red blood cell aggregation upon incubation with virus; however this technique is less sensitive and can only be used for specific viruses.¹⁰⁹ Using the device designed in aim 2 I will investigate changes in cell acoustic properties upon infection with DENV virus. The goal is to use this device to obtain quantitative information of the number of infected, healthy and nonviable cells, as well as the amount of free virus as infection progresses. In aim 3 I will investigate changes in cell impedance, deformability and optical properties upon infection to identify infected cells early after infection.

Aim 1: Applying Particle Tracking Microrheology to Sputum

Develop and optimize a quantitative method to measure heterogeneous complex biological samples.

Often samples, especially sputum, must be digested and homogenized before entering microfluidic devices.²¹ Therefore, it is necessary to quantify sputum mechanical properties on the micro-scale. I aim to apply microrheology to human sputum, and investigate methods to digest its structure.

Research Design

In order to apply particle tracking microrheology to sputum being degraded, an algorithm to remove directed motion from particle tracks has been developed. When liquefaction agents are added to sputum local currents are induced that make it impossible to use particle tracking microrheology without addressing the outside sources of movement.

To remove directed motion, movement along the axis of greatest movement is eliminated and only motion perpendicular to this axis is used to calculate rheological properties. This technique is simple, computationally efficient, theoretically sound and does not introduce complex fitting parameters. It is analogous to the method used by Hasnain et al. to analyze the anisotropy of DNA solutions,¹¹⁰ however, the de-trending algorithm will be applied to each bead trajectory individually instead of the sample as a whole. I hypothesize that by using this technique it will be possible to use particle tracking microrheology to measure heterogeneous dynamic samples.

Simulations

The error introduced using a 1D detrending algorithm has been assessed by simulated beads trajectories with and without directed motion. A particle moving in 1D due to Brownian motion alone in a purely viscous fluid can be described as

$$\rho(x, t) = \frac{1}{(4\pi Dt)^{1/2}} e^{-(x^2/4Dt)} \quad \text{Equation 3}$$

Where $\rho(x, t)$ is the probability of moving x distance in t time, and D is the diffusion constant of the environment. Thus, I simulated each step in x and y as a normal distribution centered around zero with a standard deviation of $(2Dt)^{1/2}$. Trajectories are calculated by taking the cumulative sum of the steps. According to Stokes-Einstein equation the dynamic viscosity can be calculated as:

$$\eta = \frac{K_b T}{6\pi Da} = \frac{K_b T}{\pi a} \frac{t}{\langle \Delta r^2(t) \rangle} \quad \text{Equation 4}$$

Where K_b is the Boltzmann constant, T is the temperature in Kelvin, η is the dynamic viscosity, and a is the particle radius. 1000 beads with a diameter of 0.49 μm are simulated in 27 different dynamic viscosities.

From the trajectories the MSD can be calculated as:

$$\langle \Delta r^2(t) \rangle = K \langle (x(t_i + t) - x(t_i))^2 \rangle \quad \text{Equation 5}$$

Where x represents the position perpendicular to the fitted line, and K is a scaling factor to translate to a 3 dimensional MSD. Based on the assumption that the material is isotropic on the length scale of the probe, the movement in all axes are equal. Therefore, the motion in one or two axes can be scaled to get representative three dimensional motion. For a 1D analysis $K=3$, whereas for a 2D analysis, $K=3/2$.¹¹¹ MSD is calculated for each time interval, t , and averaged over all possible initial times. As a result, smaller time intervals are averaged over more measurements. The creep compliance, $\Gamma(t)$, is calculated as:

$$\Gamma(t) = \frac{\pi a}{K_b T} \langle \Delta r^2(t) \rangle \quad \text{Equation 6}$$

Where a is the particle radius, K_b is the Boltzmann constant and T is the temperature in Kelvin. I then calculated the percent error as:

$$\frac{\text{Calculated}-\text{Theoretical}}{\text{Theoretical}} * 100 \quad \text{Equation 7}$$

The theoretical estimate is based on the simulated dynamic viscosity. The calculated estimate is based on the mean squared displacement of the particle trajectories. All percent errors are calculated from creep compliance estimates at 20 Hz. Creep compliances are reported to compare to sputum measurements, a solid-like material. Percent error, ϵ , is calculated for each bead trajectory, then the average percent error, $\bar{\epsilon}$, and corresponding standard deviation, σ , is computed for each population of 1000 simulated beads. No trend is observed between error and simulated viscosity, therefore the average percent error, $\bar{\epsilon}$, and standard deviation, σ , is averaged over the 27 different environments to get a double averaged percent error, $\bar{\bar{\epsilon}}$ and mean standard deviation $\bar{\sigma}$.

In order to simulate a broad range of directed motion, the amount of directed motion added at each step varies from 0.01 to 3 times the average displacement in one step. Since no strong relation between error and dynamic viscosity is observed, these simulations are performed for five different dynamic viscosities. The error is calculated by Equation 7. For 2D analysis with directed motion, different track lengths have similar amounts of error; therefore error is averaged again over track length.

Experimental Studies

0.49 μm diameter carboxylate-modified red fluorescent polystyrene microspheres (Invitrogen, Carlsbad, CA) will be tracked with a custom inverted confocal spinning disk microscope with a 63x objective, 1.4NA (Leica Microsystems, Wetzlar, Germany), and an electron multiplying CCD camera (Hamamatsu Photonics, Hamamatsu, Japan). Glass bottom 96-well plates (MatTek Corp., Ashland, MA) will be used for all experiments and an incubation chamber to keep the samples at 20°C (Pathology Devices, Westminster, MD). Images will be captured at 20 Hz with a 5 ms exposure time. A particle tracking algorithm developed by the Kilfoil lab at University of Massachusetts at Amherst will be used to get particle trajectories.⁴³ Longer track times give more reliable estimates of compliance since more displacements are averaged over. Thus, beads that were tracked for less than 5 seconds will be eliminated to increase accuracy.

Glycerol in water The sample is disturbed shortly before imaging by pipetting to introduce directed motion. The ensemble mean creep compliance is weighted by the track length of each trajectory.

Sputum Approximately 100ul portions of sputum have been measured for each trial, with either no (native) digestant added or aqueous NaOH added in a 1:10 ratio of NaOH to sputum. The concentration of added aqueous NaOH will be varied to obtain final concentrations of 0 to 4% w/v NaOH in sputum. Bulk digestion protocols usually involve adding NaOH in a 1:1 ratio to sputum to a final concentration of 1-2% NaOH. To facilitate mixing the NaOH was pipetted up and down in the sputum multiple times. For heterogeneous materials, the spread of the data is much more informative than an average, thus box plots will be used to display the creep compliances.

Potential challenges Our preliminary results indicate that materials with higher creep compliances are more difficult to measure with our system. Bulk digestion protocols require samples to be dilute in large amounts of PBS after digestion with NaOH, which drastically reduces sample creep compliance. In order to address this issue, I have 1) scaled down the bulk digestion protocol as discussed above and 2) measured samples without diluting them in PBS to assess the effect of the NaOH. This not

only reduced the volume of the processed sample, which is ideal for microfluidic devices that only require small amounts of sample, but also enabled us to measure the sample with our system.

Preliminary Results

Results in this section are taken from Fong et al.¹¹²

Simulations

1D de-trending significantly reduces error when convection dominates over diffusion.

Applying our de-trending algorithm to simulated data without directed motion results in slightly underestimated creep compliances, but the error does not exceed 1% when beads are tracked for 5 seconds or greater. The error is consistent across various simulated viscosities. As expected, the longer the time the bead is tracked, the less error and more consistent results are.

When the directed motion is on the same order as the Brownian motion the error in estimated creep compliance is over 40%. This error increases to over 375% average percent error for directed motion that is three times the average displacement (Figure 15a). However, with de-trending the average percent error is less than one percent even when the directed motion is three times as large as the average displacement (Figure 15b). These results indicate a one-dimensional analysis removes the directed motion and is insensitive to the amount of directed motion as seen by the overlap between different amounts of directed motion (Figure 15b and c). For directed motion that is less than 10% of the average displacement in one time step the error is negligible, < 1% average percent error, even without de-trending data (Figure 15a *inset*). When there is little directed motion, less than 10% of the average step size, the two dimensional analysis performs similarly to the one dimensional analysis. However, once the directed motion becomes larger, the creep compliance is severely overestimated when data is not de-trended.

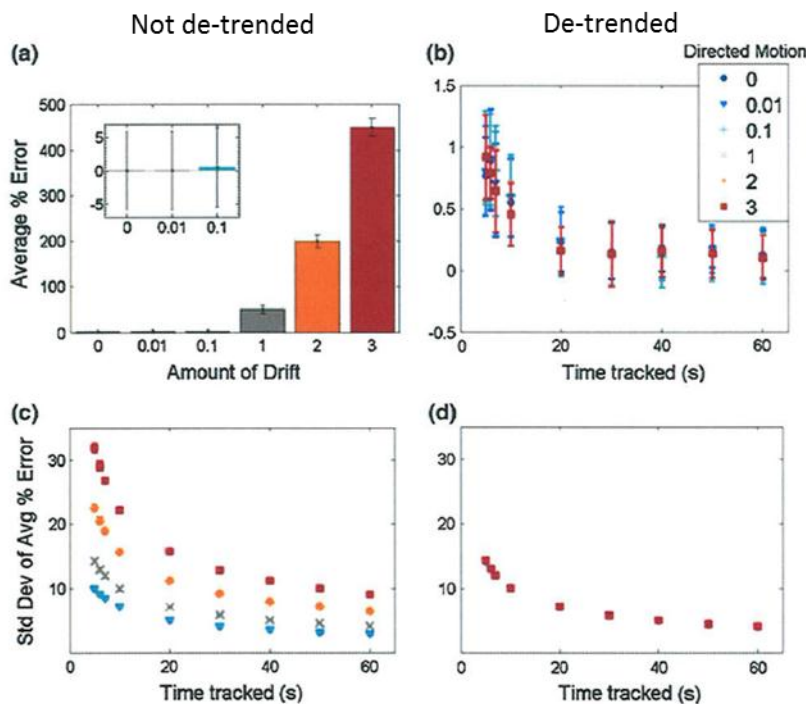


Figure 15 De-trending algorithm to remove directed motion. Percent error of creep compliance in particles with directed motion. The amount of directed motion corresponds to 0.01 to 3 times the average step size. (a) Average percent error without de-trending. The error bars correspond to the mean standard deviation

averaged over all track lengths presented in (c). (b) Average percent error after de-trending. (c) Average standard deviation without de-trending. (d) Average standard deviation after de-trending. Taken from [112]

Experimental Studies

Glycerol-water mixtures serve as a model system and different viscosities are measured.

The creep compliances of 0 to 90% glycerol in water solutions are measured with PTM. Since glycerol characteristics are well characterized, this data serves as a standard to compare with results from unknown samples. These results indicate the creep compliance estimated using particle tracking with de-trending overestimates the creep compliance as compared to tabulated values for glycerol-water solutions,¹¹³ (Figure 16a) and is consistent with data reported elsewhere.³⁵

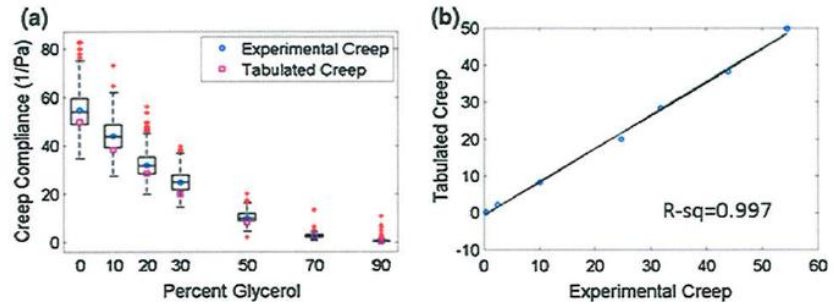


Figure 16 Creep compliance at 20 Hz of glycerol. (a) Creep compliances after de-trending. The ensemble average was calculated by weighing by track time (blue circles). Tabulated creep values were calculated from tabulated viscosities at 20Hz (magenta squares). (b) Calibration curve between averaged experimental creep compliances and tabulated values. Linear fit: $\text{Tabulated Creep} = 0.902(\text{Experimental Avg Creep}) - 0.644$, $R^2=0.997$. Mean viscosities calculated from experiments are: $9.3E-2$, $1.166E-3$, $1.599E-3$, $1.207E-3$, $5.120E-3$, 0.120 Pa s from 0 to 90% glycerol. Taken from [112].

Since both the experimental and tabulated values exhibit the same behavior with percent glycerol the system can be calibrated for purely viscous homogenous Newtonian fluids (Figure 16b).

The addition of small amounts of highly concentrated sodium hydroxide does not digest all regions of sputum samples.

Two sputum samples are measured before and after adding NaOH. NaOH is added to sputum in a 1:10 volume ratio to obtain final concentrations in the range used for bulk digestion. When NaOH is added to the sputum to a final concentration of 1 or more percent the spread of the creep compliance increases, and suggests an increase in the sample heterogeneity (Figure 17). This suggests that NaOH increases the heterogeneity of sputum by degrading portions of the microstructure of the sputum and thus dramatically increasing the creep compliance, while not affecting other portions. The maximum creep compliance increases for both sample A and B after the addition of NaOH, and the lowest observed creep compliance remains relatively equal as compared to the native samples. I hypothesize that either the NaOH loses efficacy soon after interacting with the sputum, or there are regions of sputum that NaOH cannot digest. This would result in an increase in maximum creep compliance observed while retaining the measurements of low creep compliances as in Figure 17.

The utility and broad applicability of our 1D de-trending algorithm for heterogeneous materials that are isotropic on the length scale of the probe, and experience only Brownian motion and consistent directed motion is demonstrated. While these assumptions limit the applicability of this technique, this very simplistic model shows the utility of de-trending methods and sets the foundation for future work in expanding these methods for more realistic systems. To demonstrate this method successfully eliminates directed motion, and performs with the same fidelity as traditional methods when there is no directed motion, a combination of simulation and experiments are performed. Next, it is used to probe changes in material properties of sputum, a complex fluid, with the addition of sodium hydroxide which induces directed motion. Overall, these results provide a method to analyze at the microscopic level, the behavior of complex and heterogeneous fluids.

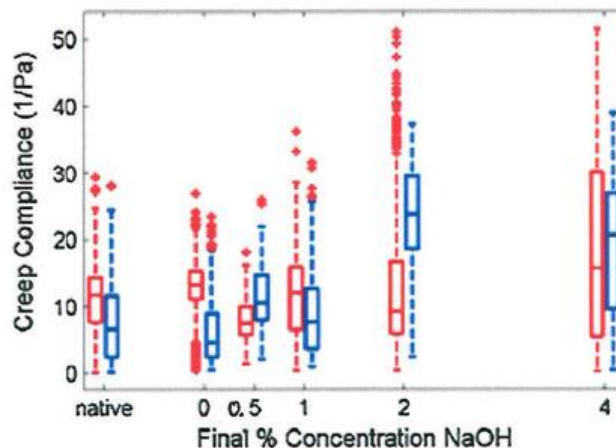


Figure 17 Creep compliance of sputum after the addition of NaOH. Adding detergent increases the variability in the creep compliance as seen by the increase in spread. Taken from [112].

These results inform how to scale bulk procedures down for processing samples for microdevices. In microfluidic devices it is often desirable to have samples that are highly concentrated with the species of interest, to increase sensitivity. These results show that minimizing the sample volume after liquefaction, by adding small amounts of highly concentrated NaOH to achieve final concentrations similar to concentrations used for bulk processing does not adequately degrade all regions of the sample. Therefore, it is important to take additional steps to homogenize the sample prior to taking a portion of it for analysis to get a representative sample. While this thesis will not pursue this avenue, a method to quantify sample homogenization and digestion has been developed. It is expected that the developed de-trending method will be useful for those trying to optimize sample degradation. This de-trending method can be used to probe complex and heterogeneous materials under dynamic conditions and can be used to evaluate sample digestion efficiency. Alternatively, using the bulk digestion protocol and focusing on sample concentration downstream may be more effective, and a method for sample purification will be discussed in the following aim.

Aim 2: Acoustofluidic Separation

Develop and optimize an acoustic separation platform to move cells from a sample stream to a clean buffer stream.

Research Design

To validate acoustic focusing through a wall different acoustic separation devices have been characterized to determine the effect of different wall widths. Next, the device will be used to investigate particle transfer between streams. Using the tools developed in this aim, I will probe cell infection with DENV. I hypothesize that the increased lipid biosynthesis induced by DENV infection in specific cell lines will result in changes in cell density and compressibility which can be probed with acoustic forces. I hypothesize that by using the device designed in this aim it will be possible to fractionate infected cells and quickly obtain a snap shot of the cell virus dynamics, by quantifying the infected, healthy, dead cells and free virus present in the culture.

Device Design

Devices will be obtained from the Lawrence Livermore National Laboratory (LLNL) sample preparation team. Channels are etched into silicon wafers and bonded anionically to glass, with a PZT piezoceramic (Piezo Systems type PSI-5A4E) glued to the silicon side with cyanoacrylate. Two channels (separation and bypass) are separated by a wall. During device operation, sample and buffer solutions are injected into the separation channel, and the bypass channel is filled with water (Figure 18). Chips operate at the second harmonic, to reduce the power required to generate acoustic forces by operating at a higher frequency. Two wall locations ($w_{SEP}=750$ and $w_{SEP}=650$ μm) will be tested. To test the effect of wall thickness, beads are injected into the inlet farthest away from the bypass channel such that the particles will focus to the pressure node (Figure 15, Generation 1).

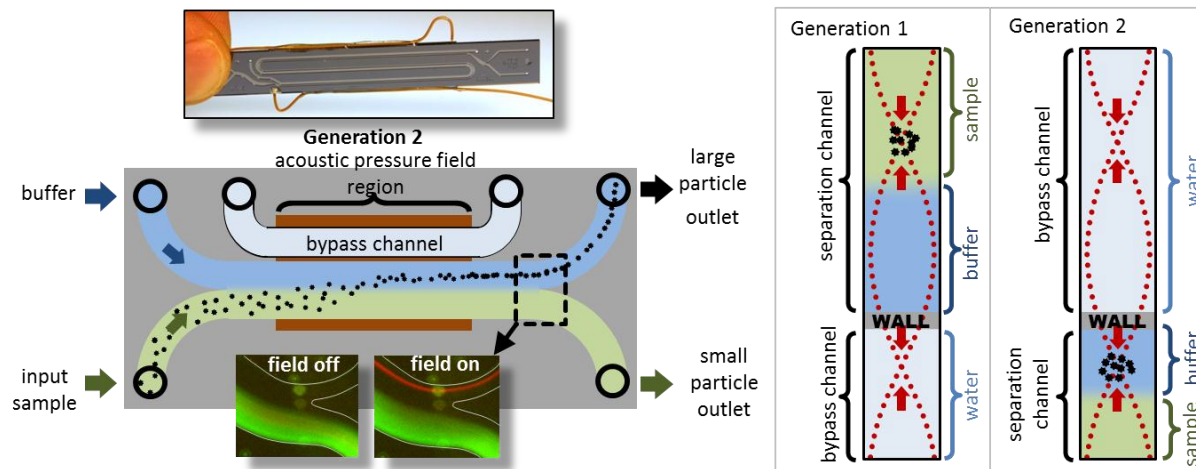


Figure 18 Left: Schematic of our acoustophoretic separation device, not to scale (Generation 2). Right: Generation 1 devices were designed to study the effect of wall thickness on focusing, and generation 2 devices were designed to transfer particles from the input stream to the buffer stream.

Second generation devices achieve separation of different sized particles by operating in the smaller channel where the acoustic force is always directed towards the same node (Figure 18, Generation 2). The sample solution is input on the side farthest from the focusing position, and the large particles migrate into the buffer stream and are extracted in the large particle outlet (LPO), while smaller particles do not experience sufficient acoustic force to move them into the buffer stream and exit in the small particle outlet (SPO). To increase the amount of time particles are in the acoustic field and enable high throughput separation, the length of the channel was increased using a serpentine design with up to three passes. Device consistency will be evaluated using approximately 120 mm long (3-pass) devices with main channel widths of $w_{SEP}=300$ and $w_{SEP}=280\mu\text{m}$, and 40mm long (single pass) devices with $300\mu\text{m}$ wide main channels. Flow restrictors at the outlet will be used to enhance particle concentration and make the system robust against flow disturbances.

Since high frequency excitation of the piezoelectric bounded to the chip induces significant heating a small fan is attached on top of the device to regulate temperature. The temperature is estimated at $30\text{-}40^\circ\text{C}$ based on an attached thermocouple.

Calibration

To find the optimal focusing frequency in first generation devices, LabView will be used to perform a frequency sweep (Agilent 33220A) with a 20V peak to peak signal and capture fluorescent images (CoolSnap, HQ2) of a 0.01% (w/v) bead solution of 5.78 μm

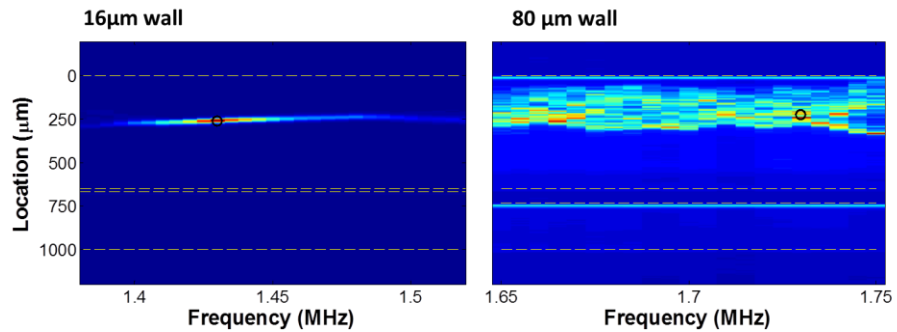


Figure 19 Representative frequency sweeps for 16 μm (left) and 80 μm (right) devices, wall is located at 650 μm . Blue is low intensity and red is high intensity. The focusing efficiencies are 0.901 and 0.294 respectively. Peak frequencies and locations are indicated by a black circle, and channel walls are indicated by dashed yellow lines.

fluorescent polystyrene beads (Bangs Laboratory) flowing at an average linear speed of 6 mm/s through the main channel. Image analysis will be performed using Matlab to determine the optimal (peak) frequency by finding the frequency with the greatest absolute intensity. Intensities are averaged over the channel length for each frequency (Figure 19). The peak frequency is determined by the maximum intensity amplitude since it is less sensitive to non-Gaussian profiles caused by stuck beads, and reduces computation time since no fitting is involved. The intensity profile at the peak frequency is fit to a Gaussian curve to find the peak location. For generation two devices, a Gaussian fit is used to determine the full width half max. Generation one devices exhibit various modes of focusing, resulting in non-Gaussian intensity profiles, therefore the focusing efficiency rather than the full width half max of the Gaussian fit is reported. The focusing efficiency is calculated as the intensity within $\pm 25\mu\text{m}$ of the peak location divided by the total intensity of the channel.

For generation 2 devices a frequency sweep is run to determine the peak frequency for each device, and then multiple measurements are performed at the peak frequency for linear flow rates of 20 and 60mm/s at different voltages to evaluate the consistency of the devices.

The focusing of different sized beads is evaluated in a generation 2, 3-pass device. Percent extracted is calculated as: $\frac{\# \text{ particles collected in LPO}}{\# \text{ particles collected from both outlets}} * 100$. A flow cytometer (Microcyte, Aber Instruments, Wales) and a coulter counter (Z2, Beckman Coulter) will be used to count beads and quantify cells, respectively.

Cell-Virus Separations

Human Raji cells are cultured in RPMI 1640 growth media supplemented with 10% fetal bovine serum at 37°C and 5% CO₂. Cells are re-suspended in 1xPBS for experiments and used within the same day. Cells are kept at room temperature during experiments. Live DENV II will be obtained at an estimated concentration of $1.2 \cdot 10^8$ plaque forming units/ml and diluted to about 1:1000 into either 1x PBS (virus only experiments) or Raji cells (spiked experiments). The virus is spiked into the cell solution shortly before performing cell separations such that the virus and cells are together less than 20 minutes before entering the separation channel. Significant cell infection is not expected to occur during this short period, but viruses may adhere to cell membranes. DENV has been shown to infect Raji cells.¹¹⁴ Fresh cell media is used to coat the device and tubing prior to running separation tests to prevent the cells and viruses from being adsorbed to tubing and chip surfaces. Reverse transcriptase PCR is used to quantify viral separation. Separation experiments are performed at flow speeds of 60mm/s, and at 16V to enable high speed extraction of cells into the clean buffer stream. Pure virus and cell samples as well as virus

spiked in cell samples are run through the chip with (16V) and without (0V) the acoustic field turned on (N=3).

Virus Infection Monitoring

The preliminary results suggest that this device can isolate cells and free virus with less effect on cell virus dynamics than centrifugation since cells are only exposed to the acoustic field for a matter of seconds, in comparison to minutes in centrifugation. To investigate the ability of the device to monitor cell virus dynamics, cells and DENV will be cultured together and at specific time points aliquots of the culture will be run through the chip and the outputs quantified.

- Free virus: Quantifying changes in the amounts of virus exiting the chip will give a measure of cell infection as more viruses will exit in the LPO in infected cells.
- Infected cells: It is expected cells will behave differently in the acoustic field, as their membrane and internal composition changes upon infection. DENV has been shown to increase lipid biosynthesis in numerous cell lines^{103,115} which should change the cell acoustic properties.⁵⁴ Preliminary results indicate that by tuning the operating voltage, different species can be isolated.
- Healthy and Non-viable cells: Prior work indicates that acoustic forces can be used to discriminate between viable and non-viable cells.⁵⁵

Quantifying the healthy, infected and dead cell populations and the free virus will give a representative picture of virus infection. In this aim I plan to establish our device as a tool to quickly obtain a picture of the cell virus dynamics, and use it to study DENV infection.

Preliminary Results

Focusing Through the Wall

Thicker walls result in higher resonant frequencies, and lower focusing efficiencies.

The equivalent water width of the silicon walls can be estimated using the relative speed of sound in silicon and water. Since the speed of sound in silicon is approximately 6 times faster than in water, thicker walls reduce the effective channel width resulting in higher resonant frequencies, and smaller nodal spacing. Resonant frequency can be calculated as: $f = \frac{nc}{2w}$. Where n is the number of pressure nodes (2 for our device), c is the speed of sound in water, and w is the equivalent channel water width of the device.

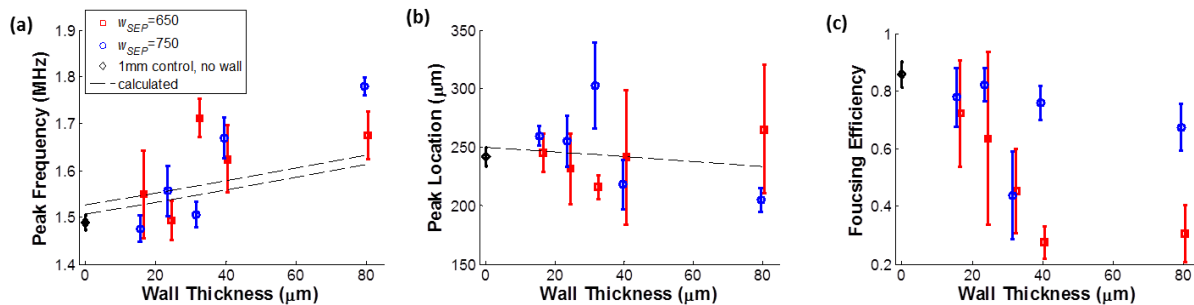


Figure 20 Peak Frequency (a), location (b), and focusing efficiency (c) for different wall widths and wall locations. Black dotted lines are theoretical calculations based on the speed of sound in silicon and water. (a) Upper dotted line is calculated 40°C, and lower theoretical line is at 30°C. (b) Differences in theoretical peak locations at 30 and 40°C were insignificant.

As predicted, the peak focusing frequency increases as the wall thickness increases, regardless of the wall location. However, this simple estimation does not capture the complexities of the physical system, and underestimates the peak frequency when compared to experimental data for wall widths greater than 32μm (Fig 20a). As the wall width increases, the focusing efficiency and peak location

become more erratic. However with wall widths of 16 μm the focusing efficiency for both 650 and 750 devices were relatively high and the focusing position is reasonably well defined. Thus, achieving acoustic focusing through thin walls appears to be possible.

Device Optimization

Optimizing field strength, flow rate, and particle size: Increasing the time particles are exposed to the acoustic field increases separation efficiency.

The location of the wall in second generation devices did not significantly change device properties. By increasing the channel length or decreasing flow speed it is possible to achieve focusing at lower voltages. The shift of the location plot for the single pass device downwards with respect to the three pass device indicates the single pass device is less efficient at focusing, since beads require higher voltages to migrate (Figure 21). Additionally, the focusing width for the single pass device is shifted up with respect to the 3-pass device, signifying that at the same power particles are less focused in the single pass device (Figure 21). A similar trend is observed when comparing the location and focusing width for the high and low flow speeds. The data points for 0V do not show a difference between the single pass and multiple pass, indicating using a serpentine design does not introduce significant mixing to degrade separation abilities at flow speeds up to 60mm/s.

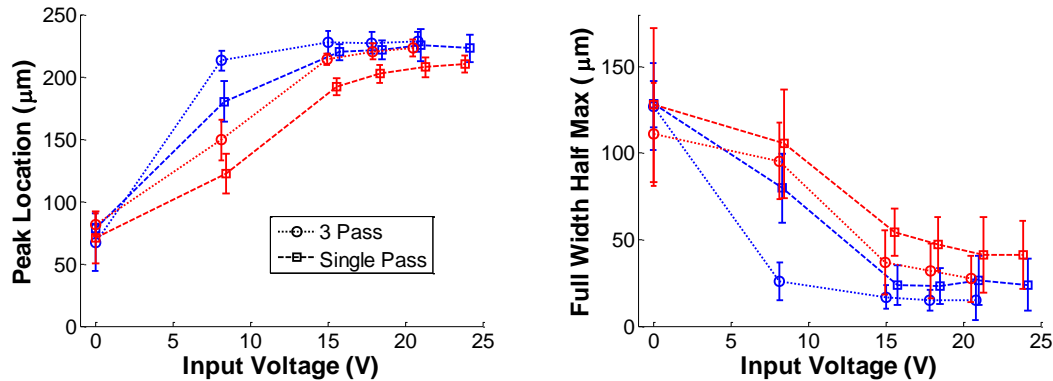


Figure 21 Peak location and width for generation 2 devices. Red: 60mm/s, Blue 20mm/s

The separation efficiency of our devices is evaluated with multiple sizes of beads at different operating voltages at flow speeds of 60mm/s. Using this data as a calibration curve the required voltages to extract particles of a particular size can be estimated (Figure 22). Since Raji cells are estimated to be 5-8 μm in diameter,¹¹⁶ I choose to operate at 16V for cell-virus separations.

Cell-Virus Separations

Cells are extracted into a clean buffer stream with greater than 95% efficiency.

Without the acoustic field turned on the cells and virus both exit in the sample stream with little diffusion, less than 2% of cells or virus exit in the clean buffer stream. With the field turned on, cells are successfully moved to the clean buffer stream, percent extracted >95% (Figure 23). However, the virus is also more likely to travel to the clean buffer stream when cells are present in the solution. Without cells 90% of viruses exit in desired outlet, the SPO, and with cells 68% exit in the SPO. By enabling arbitrary node placement cell-virus separation is achieved with higher cell extraction and at greater than tenfold speeds than existing microfluidic devices.⁵⁷

Next, the reason for drop in virus separation from approximately 90% to 70% when cells are present will be investigated. The amount of free virus moving into the buffer stream must be minimized for optimal device function.

I will quantify infection progression by measuring cell-virus cultures at different time points post infection. Based on existing work characterizing DENV infection in cells,¹¹⁷ the number of viruses exiting in the LPO is expected to be relatively low immediately after cells are infected, and then increase as cells are being infected. Infected cells will move the viruses within them into the LPO. The infection rate will plateau, and then a second round of infection will occur as the proliferated virus is released from cells into the media. When the second round of infection occurs I expect to see an increase in the total amount of virus (in both the SPO and LPO).

Virus Infection Monitoring: Potential challenges and strategies

Free virus appears to move with the cells into the buffer stream. Completely eliminating free virus transfer into the buffer stream may be impossible due to increased mixing caused by cells crossing fluid streamlines. I will use inert model cells (ie beads) to determine the amount of transfer purely due to large particles changing streamlines. Depending on results, I will investigate using more realistic models, such as artificial liposomes,¹¹⁸ or cells with surface receptors blocked. Additionally, samples may be run through the chip multiple times to enhance cell washing and to understand the efficiency of the device at different virus concentrations. It is expected that as the sample is run through the chip multiple times, virus transfer into the buffer stream should decrease as the free virus is washed from the cells, and then plateau when only the virus associated with cells remain.

Model system to determine if it is possible to identify virus infected cells. It is possible that DENV infected cells will not be distinguishable using acoustic forces. While evidence of changes in cell

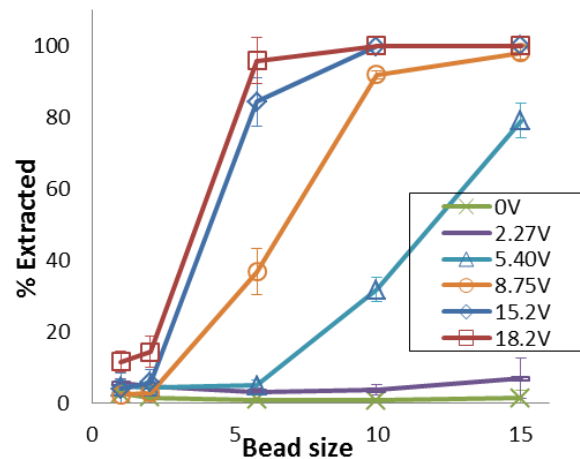


Figure 22 Recovery of particles from large particle outlet. Each data point is averaged over three trials, error bars are one standard deviation.

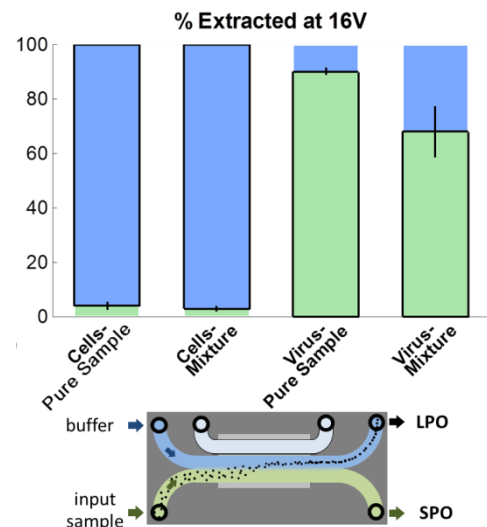


Figure 23 Percent extracted in blue: large particle outlet (clean buffer stream) and green: small particle outlet at 16V for pure cell and virus samples and for cells spiked with virus.

metabolism suggests that the acoustic properties of the cells will change upon infection, this change may not be significant enough for the device to isolate infected cells. To determine the limit of resolution for the device, I plan to use a model cells to controllably change “cell” properties. Droplet microfluidics has been used to reliably manufacture liposomes, by creating droplets with a lipid bilayer.¹¹⁸ Using this technique, it is possible to make artificial cells and control the interior composition. Alternative approaches include using the acoustic device to distinguish cells derived from adipose tissue versus other types of cells to determine if lipid content changes cell acoustic properties.

While the acoustic device may have a limited ability to distinguish newly infected cells, it is expected as significant changes occur, cell acoustic properties will change and infected cells will be distinguishable. However, being able to identify infected cells before significant metabolic and physical changes occur is desirable. Therefore there is significant interest in investigating techniques that can probe the cell interior, which will be addressed in aim 3.

Aim 3: Single Cell Impedance and Mechanics

Investigate cell impedance in relation to mechanical and optical form and function.

Research Design

In order for impedance spectroscopy to become accepted as a way to probe cells it is necessary to establish a relationship between cell impedance and cell state. The work with sputum in aim 1 highlights two key facts that help us attack this problem. Heterogeneity in sputum on the micro-scale isn't observable by bulk measurements. In order to obtain the resolution needed to interrogate cells, 1. measurements must be taken at relevant length scales: the single cell level, and 2. heterogeneity between cells must be accounted for. To probe changes in cell state despite inherent cell heterogeneity, the goal is to enable single cell measurements on **the same cell** over time. Correlating impedance measurements with multiple cell physical properties such as size, deformability and optical properties will make cell impedance a more accessible parameter. Cell mechanical properties have been shown to be essential in cell function,⁹² and different cell lines^{82,83,119} and cell states¹³ exhibit different mechanical properties. By maintaining optical access to the cells, impedance measurements can be related to well-studied and accepted optical markers. I hypothesize that lipid and membrane rearrangement^{103,115} caused by DENV infection will reduce the cell's impedance and increase its deformability.

Drawing inspiration from previous reports of hydrodynamic cell trapping^{93,120}, single cell impedance spectroscopy⁸¹, and dielectrophoretic cell manipulation^{87,88,95} a device that can concurrently probe cells in the mechanical, electrical and optical domains will be developed. For long term time-resolved studies, single-cells must be retained in place or repeatedly pass through a measurement site. To achieve this, physical capture structures used in hydrodynamic capture arrays and 3-D electrodes used for impedance spectroscopy will be combined. A physical trapping site made of angled 3-D electroplated electrodes will trap cells for interrogation. This configuration allows high sensitivity impedance measurements by establishing good electrical contact between the cells and electrodes.

To perform stiffness studies, the 3-D electrodes will be supplemented by a planar electrode to impose forces for electrodeformation measurements (Figure 24). Electrodeformation has been chosen to measure cell deformability for multiple reasons. It does not require physical trapping and squeezing of cells, like micropipette aspiration, which may increase device fouling and limit the lifetime of the device. Other methods such as optical stretching will increase device fabrication complexity, by requiring a laser set up. The ultimate vision for this technology is to scale it up to an array of capture sites which can monitor cell properties over time. Therefore, the stable capture of cells is paramount, and methods measuring cell properties in flow were not considered.

During electrodeformation measurements cells will move towards the small planar electrode where the electric field is highest. Particles will not be physically constrained by the capture and impedance structures in this mode, allowing for accurate whole cell deformability to be measured (Figure 24). Electrical forces generated by the electrodes are also useful for unloading a cell from the trapping site.

It is anticipated that using hydrodynamic traps will allow greater measurement flexibility and improved cell viability as compared to cell manipulation by DEP alone. A limitation of DEP is that trapping forces depend strongly on the conductivity of the suspending medium. Holding the cell with a hydrodynamic capture structure allows for easy replacement of suspending media with low conductivity fluid during deformation measurements to increase the DEP force and reduce electrical stress on the cell by reducing the voltage drop across the cell membrane.⁸⁷ During electrodeformation measurements cells will be suspended in low conductivity, iso-osmotic sugar solution. To limit the negative effects of this non-physiological medium, cells will be re-suspended in media as soon as deformation measurements finished. Media exchange capability will become essential as the device is scaled up to large arrays of measurement sites. It will enable cells to be cultured on chip and probed with chemical stimuli.⁷⁸

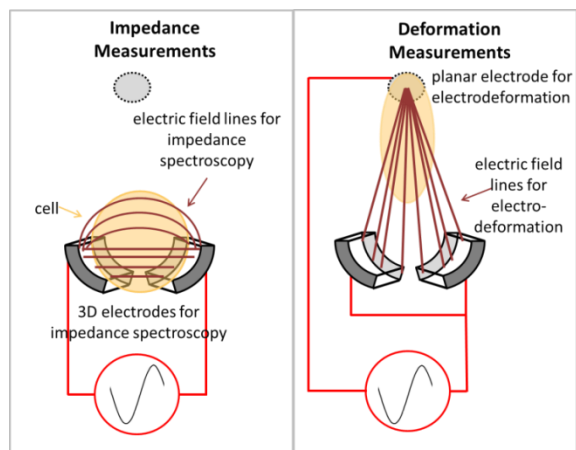


Figure 24 Schematic of proposed device for electric interrogation.

Media exchange capability will become essential as the device is scaled up to large arrays of measurement sites. It will enable cells to be cultured on chip and probed with chemical stimuli.⁷⁸

Potential Challenges and Strategies

Device Design While I expect the cells to have good electrical contact with the 3-D electrodes, it is possible that leakage current may limit the ability of impedance spectroscopy to probe cell electrical properties, and measurements will be dominated by cell size. By suspending cells in low conductivity media, I hope to minimize the leakage current. In order to further normalize by cell size I will measure cell impedance at a high and low frequency, as well as measure cell size via optical measurements. I hope that having optical access to cells will aid in device troubleshooting and in interpreting data.

Model Biological System I can validate the system with existing cell lines and treated cells that have been shown to change their mechanical and electrical properties. By making the cell membrane permeable using chemical reagents or toxins, I expect to see a decrease in cell impedance.⁷⁸ Additionally, by fixing cells using paraformaldehyde I can increase the cell stiffness and quantify the systems' ability to measure changes in cell deformability. An alternative approach is to fabricate artificial cells and control the cell interior.¹¹⁸ For example, Hur et al.¹²¹ use viscous oil droplets and elastic particles to quantify the effect of different particle viscoelastic properties, and use these results design a device to separate cancerous cells from blood. While it is possible that some DENV infected cells will not show changes in impedance or deformability, existing work suggests that endothelial infected cells will show changes in impedance.¹²²

While components of the proposed device have been implemented previously, integrating these different modes of measurements promises to generate new insights and requires a completely different device design. Being able to detect virus infected cells before they outwardly show signs of infection, such as changes in cell morphology or viral budding occurs, will be extremely useful to study early infection dynamics. This system will be used to measure cells and DENV infected cells. DENV infection increases endothelial cell permeability which changes their electrical properties,¹²² therefore this

cell line will be considered as model system for studying DENV infection. Collaborators at LLNL have extensive knowledge about DENV infection and will be able to assist in troubleshooting and interpreting results in the biological domain.

Expected Results

Changes in cell impedance spectra are expected to occur at high frequencies in DENV infected cells before infection is apparent by cytopathic effects. Infection with DENV has been shown to induce rearrangement and expansion of the endoplasmic reticulum early after infection (approximately 12 hours post infection).¹²³ This rearrangement is expected to change the cytoplasm impedance. Additionally, impedance measurements at moderate frequencies are expected to change as dengue infection changes cell membrane properties. Increases epithelial cell permeability upon DENV infection have been shown to decrease measured impedance.¹²² DENV also causes an increase in the total surface area of the cell membrane as it induces membrane curvature and establishes reaction centers where the virus is synthesized.¹¹⁵ As the infection progresses it is hypothesized that changes in cell impedance spectra at lower frequencies will be observed as the virus affects the cell health and cell apoptosis begins.

Conclusion

In conclusion, this project will address three challenges in utilizing microfluidic devices for biological sample preparation. Our first two aims address two alternative ways to approach sample preparation. First, I focus on methods to quantify sample quality. Adapting PTM to quantitatively measure viscous samples that are not at equilibrium will provide measurements more relevant to micro-devices and accelerate the optimization of sample digestion protocols. Optimizing sample digestion reduces the need for complex sample preparation procedures to be performed on chip and will make current devices accessible to a range of complex biological samples. Next, I focus on sample purification on chip using our innovative acoustic device. Using a thin wall to subdivide the channel and position cells arbitrarily using acoustic forces dramatically expands the potential of acoustophoretic manipulation, a well-established cell handling platform. By attacking the challenge of extracting desired species from both the sample rheology side, and the sample purification side, I hope to provide tools that will facilitate the use of microfluidics for a variety of difficult biological samples. Finally, the need for function specific, non-invasive biomarkers for cell identification will be considered. By correlating changes in cell state to their impedance spectra, deformability, size and optical measurements, it will be possible to see novel associations between these properties. This will allow deeper exploration of how biological structure predicts function, and impedance spectra to be more widely implemented for cell sensing. It will immediately enable novel assays to be performed investigating changes in cell physical properties with changes in cell state, and ultimately spur the development and adoption of innovative cytometers. While each aim is distinct, together they promise to enable complex clinical samples to be interrogated with single cell resolution on microfluidic platforms.

Acknowledgements

This work performed under the auspices of the U.S. Department of Energy by Lawrence Livermore National Laboratory under Contract DE-AC52-07NA27344.

References

1. Guck, J. *et al.* The optical stretcher: a novel laser tool to micromanipulate cells. *Biophys J* **81**, 767–784 (2001).
2. Gossett, D. R. *et al.* Hydrodynamic stretching of single cells for large population mechanical phenotyping. *PNAS* **109**, 7630–7635 (2012).
3. Antia, M., Herricks, T. & Rathod, P. K. Microfluidic Modeling of Cell–Cell Interactions in Malaria Pathogenesis. *PLoS Pathog* **3**, e99 (2007).
4. Grover, W. H. *et al.* Measuring single-cell density. *PNAS* (2011). doi:10.1073/pnas.1104651108
5. Hartono, D. *et al.* On-chip measurements of cell compressibility via acoustic radiation. *Lab Chip* **11**, 4072–4080 (2011).
6. Yeo, L. Y., Chang, H.-C., Chan, P. P. Y. & Friend, J. R. Microfluidic Devices for Bioapplications. *Small* **7**, 12–48 (2011).
7. Kim, J., Johnson, M., Hill, P. & Gale, B. K. Microfluidic sample preparation: cell lysis and nucleic acid purification. *Integrative Biology* **1**, 574 (2009).
8. Ritzi-Lehnert, M. Development of chip-compatible sample preparation for diagnosis of infectious diseases. *Expert Review of Molecular Diagnostics* **12**, 189–206 (2012).
9. Song, S. & Singh, A. K. On-chip sample preconcentration for integrated microfluidic analysis. *Anal Bioanal Chem* **384**, 41–43 (2006).
10. Gossett, D. R. *et al.* Label-free cell separation and sorting in microfluidic systems. *Anal Bioanal Chem* **397**, 3249–3267 (2010).
11. Sieuwerts, A. M. *et al.* Anti-Epithelial Cell Adhesion Molecule Antibodies and the Detection of Circulating Normal-Like Breast Tumor Cells. *JNCI Journal of the National Cancer Institute* **101**, 61–66 (2008).
12. Sun, T., Green, N. & Morgan, H. Analytical and Numerical Modeling Methods for Impedance Analysis of Single Cells On-Chip. *Nano* **03**, 55–63 (2008).
13. Carlo, D. D. A Mechanical Biomarker of Cell State in Medicine. *Journal of Laboratory Automation* **17**, 32–42 (2012).
14. Hou, H. *et al.* Microfluidics for Applications in Cell Mechanics and Mechanobiology. *Cellular and Molecular Bioengineering* **4**, 591–602 (2011).
15. Niemz, A., Ferguson, T. M. & Boyle, D. S. Point-of-care nucleic acid testing for infectious diseases. *Trends in Biotechnology* **29**, 240–250 (2011).
16. Cho, Y.-K. *et al.* One-step pathogen specific DNA extraction from whole blood on a centrifugal microfluidic device. *Lab Chip* **7**, 565–573 (2007).
17. Etzkorn, J. R., McQuaide, S. C., Anderson, J. B., Meldrum, D. R. & Parviz, B. A. Forming Self-Assembled Cell Arrays and Measuring the Oxygen Consumption Rate of a Single Live Cell. *Dig Tech Papers* **2009**, 2374–2377 (2009).
18. Zhao, Y. *et al.* A microfluidic system for cell type classification based on cellular size-independent electrical properties. *Lab Chip* **13**, 2272–2277 (2013).
19. Lai, S. K., Wang, Y.-Y., Wirtz, D. & Hanes, J. Micro- and macrorheology of mucus. *Advanced Drug Delivery Reviews* **61**, 86–100 (2009).
20. Govindarajan, A. V., Ramachandran, S., Vigil, G. D., Yager, P. & Böhringer, K. F. A low cost point-of-care viscous sample preparation device for molecular diagnosis in the developing world; an example of microfluidic origami. *Lab Chip* **12**, 174–181 (2012).
21. Cepheid. Xpert MTB/RIF Brochure. (2009).
22. Gubala, V., Harris, L. F., Ricco, A. J., Tan, M. X. & Williams, D. E. Point of care diagnostics: status and future. *Analytical chemistry* **84**, 487–515 (2011).
23. Lee, H., Sun, E., Ham, D. & Weissleder, R. Chip–NMR biosensor for detection and molecular analysis of cells. *Nature Medicine* **14**, 869–874 (2008).
24. Isenberg, H. D. *Essential Procedures for Clinical Microbiology*. (ASM Press, 1998).

25. Kent, P. T. & Centers for Disease Control (U.S.). *Public health mycobacteriology: a guide for the level III laboratory*. (U.S. Dept. of Health and Human Services, Public Health Service, Centers for Disease Control, 1985).
26. Steingart, K. R. *et al.* Sputum processing methods to improve the sensitivity of smear microscopy for tuberculosis: a systematic review. *The Lancet Infectious Diseases* **6**, 664–674 (2006).
27. Yamada, H., Mitarai, S., Aguiman, L., Matsumoto, H. & Fujiki, A. Preparation of mycobacteria-containing artificial sputum for TB panel testing and microscopy of sputum smears. *The International Journal of Tuberculosis and Lung Disease* **10**, 899–905 (2006).
28. Peres, R. L. *et al.* Comparison of two concentrations of NALC-NaOH for decontamination of sputum for mycobacterial culture [Technical note]. *The International Journal of Tuberculosis and Lung Disease* **13**, 1572–1575 (2009).
29. Mahalanabis, M., Do, J., ALMuayad, H., Zhang, J. Y. & Klapperich, C. M. An integrated disposable device for DNA extraction and helicase dependent amplification. *Biomed Microdevices* **12**, 353–359 (2010).
30. Zhang, J. *et al.* A Disposable Microfluidic Virus Concentration Device Based on Evaporation and Interfacial Tension. *Diagnostics* **3**, 155–169 (2013).
31. Alam, M. M. & Mezzenga, R. Particle tracking microrheology of lyotropic liquid crystals. *Langmuir : the ACS journal of surfaces and colloids* **27**, 6171–8 (2011).
32. Valentine, M. T. *et al.* Investigating the microenvironments of inhomogeneous soft materials with multiple particle tracking. *Physical Review E* **64**, 061506 (2001).
33. Mason, T. G., Ganesan, K., Van Zanten, J. H., Wirtz, D. & Kuo, S. C. Particle tracking microrheology of complex fluids. *Physical Review Letters* **79**, 3282–3285 (1997).
34. Rogers, S. S., Waigh, T. a & Lu, J. R. Intracellular microrheology of motile Amoeba proteus. *Biophysical journal* **94**, 3313–22 (2008).
35. Apgar, J. Multiple-Particle Tracking Measurements of Heterogeneities in Solutions of Actin Filaments and Actin Bundles. *Biophysical Journal* **79**, 1095–1106 (2000).
36. Baker, E. L., Bonnecaze, R. T. & Zaman, M. H. Extracellular Matrix Stiffness and Architecture Govern Intracellular Rheology in Cancer. *Biophysical Journal* **97**, 1013–1021 (2009).
37. Gal, N. & Weihs, D. Intracellular Mechanics and Activity of Breast Cancer Cells Correlate with Metastatic Potential. *Cell Biochemistry and Biophysics* (2012). doi:10.1007/s12013-012-9356-z
38. Crocker, J. C. & Hoffman, B. D. Multiple-particle tracking and two-point microrheology in cells. *Methods in cell biology* **83**, 141–78 (2007).
39. Wirtz, D. Particle-tracking microrheology of living cells: principles and applications. *Annual review of biophysics* **38**, 301–26 (2009).
40. Suh, J., Dawson, M. & Hanes, J. Real-time multiple-particle tracking: applications to drug and gene delivery. *Advanced Drug Delivery Reviews* **57**, 63–78 (2005).
41. Tseng, Y., Kole, T. P. & Wirtz, D. Micromechanical mapping of live cells by multiple-particle-tracking microrheology. *Biophysical journal* **83**, 3162–76 (2002).
42. Weihs, D., Teitell, M. a. & Mason, T. G. Simulations of complex particle transport in heterogeneous active liquids. *Microfluidics and Nanofluidics* **3**, 227–237 (2006).
43. Pelletier, V., Gal, N., Fournier, P. & Kilfoil, M. Microrheology of Microtubule Solutions and Actin-Microtubule Composite Networks. *Physical Review Letters* **102**, 100–103 (2009).
44. Dangaria, J., Yang, S. & Butler, P. Improved nanometer-scale particle tracking in optical microscopy using microfabricated fiduciary posts. *BioTechniques* **42**, 437–440 (2007).
45. Laurell, T., Petersson, F. & Nilsson, A. Chip integrated strategies for acoustic separation and manipulation of cells and particles. *Chemical Society Reviews* **36**, 492 (2007).
46. Gossett, D. R. *et al.* Inertial Manipulation and Transfer of Microparticles Across Laminar Fluid Streams. *Small* **8**, 2757–2764 (2012).
47. Mach, A. J., Kim, J. H., Arshi, A., Hur, S. C. & Carlo, D. D. Automated cellular sample preparation using a Centrifuge-on-a-Chip. *Lab Chip* **11**, 2827–2834 (2011).

48. Augustsson, P., Persson, J., Ekström, S., Ohlin, M. & Laurell, T. Decomplexing biofluids using microchip based acoustophoresis. *Lab on a Chip* **9**, 810 (2009).
49. Burguillos, M. A. *et al.* Microchannel Acoustophoresis does not Impact Survival or Function of Microglia, Leukocytes or Tumor Cells. *PLoS ONE* **8**, e64233 (2013).
50. Jung, B., Fisher, K., Ness, K. D., Rose, K. A. & Mariella, R. P. Acoustic Particle Filter with Adjustable Effective Pore Size for Automated Sample Preparation. *Anal. Chem.* **80**, 8447–8452 (2008).
51. Petersson, F., Nilsson, A., Holm, C., Jönsson, H. & Laurell, T. Continuous separation of lipid particles from erythrocytes by means of laminar flow and acoustic standing wave forces. *Lab on a Chip* **5**, 20 (2005).
52. Petersson, F., Aberg, L., Swärd-Nilsson, A.-M. & Laurell, T. Free flow acoustophoresis: microfluidic-based mode of particle and cell separation. *Anal. Chem.* **79**, 5117–5123 (2007).
53. Augustsson, P., Magnusson, C., Nordin, M., Lilja, H. & Laurell, T. Microfluidic, Label-Free Enrichment of Prostate Cancer Cells in Blood Based on Acoustophoresis. *Analytical Chemistry* **84**, 7954–7962 (2012).
54. Petersson, F., Nilsson, A., Holm, C., Jönsson, H. & Laurell, T. Separation of lipids from blood utilizing ultrasonic standing waves in microfluidic channels. *Analyst* **129**, 938–943 (2004).
55. Yang, A. H. J. & Soh, H. T. Acoustophoretic Sorting of Viable Mammalian Cells in a Microfluidic Device. *Anal Chem* (2012).
56. Hawkes, J. J., Barber, R. W., Emerson, D. R. & Coakley, W. T. Continuous cell washing and mixing driven by an ultrasound standing wave within a microfluidic channel. *Lab on a Chip* **4**, 446 (2004).
57. Zhao, C. & Cheng, X. Microfluidic separation of viruses from blood cells based on intrinsic transport processes. *Biomicrofluidics* **5**, 032004–032004–10 (2011).
58. Leland, D. S. & Ginocchio, C. C. Role of Cell Culture for Virus Detection in the Age of Technology. *Clinical Microbiology Reviews* **20**, 49–78 (2007).
59. Darlin, D. *et al.* Low-speed centrifugation of retroviral vectors absorbed to a particulate substrate: a highly effective means of enhancing retroviral titre. , *Published online: 25 May 2000; / doi:10.1038/sj.gt.3301201* **7**, (2000).
60. Sundin, D. R. & Mecham, J. O. Enhanced infectivity of bluetongue virus in cell culture by centrifugation. *J. Clin. Microbiol.* **27**, 1659–1660 (1989).
61. Brody, J. & Yager, P. Low Reynolds number micro-fluidic devices. *Proc. of Solid-State Sensor and Actuator Workshop* 105–108 (1996).
62. Glynne-Jones, P., Boltryk, R. J., Harris, N. R., Cranny, A. W. J. & Hill, M. Mode-switching: A new technique for electronically varying the agglomeration position in an acoustic particle manipulator. *Ultrasonics* **50**, 68–75 (2010).
63. Doblhoff-Dier, O. *et al.* A novel ultrasonic resonance field device for the retention of animal cells. *Biotechnol. Prog.* **10**, 428–432 (1994).
64. McSharry, J. J. Uses of flow cytometry in virology. *Clin. Microbiol. Rev.* **7**, 576–604 (1994).
65. Cheng, X. *et al.* A microfluidic device for practical label-free CD4+ T cell counting of HIV-infected subjects. *Lab Chip* **7**, 170–178 (2007).
66. Dharmasiri, U. *et al.* High-Throughput Selection, Enumeration, Electrokinetic Manipulation, and Molecular Profiling of Low-Abundance Circulating Tumor Cells Using a Microfluidic System. *Anal. Chem.* **83**, 2301–2309 (2011).
67. Gorges, T. M. *et al.* Circulating tumour cells escape from EpCAM-based detection due to epithelial-to-mesenchymal transition. *BMC Cancer* **12**, 178 (2012).
68. Cheung, K., Gawad, S. & Renaud, P. Impedance spectroscopy flow cytometry: On-chip label-free cell differentiation. *Cytometry Part A* **65A**, 124–132 (2005).
69. Gawad, S., Schild, L. & Renaud, P. Micromachined impedance spectroscopy flow cytometer for cell analysis and particle sizing. *Lab Chip* **1**, 76–82 (2001).

70. Liu, C.-F., Chen, M.-K. & Jang, L.-S. Design and fabrication of coplanar waveguide probes for single-cell impedance measurement using radio frequency. *IET Micro Nano Letters* **6**, 503–509 (2011).
71. Myers, F. B., Zarins, C. K., Abilez, O. J. & Lee, L. P. Label-free electrophysiological cytometry for stem cell-derived cardiomyocyte clusters. *Lab on a Chip* **13**, 220 (2013).
72. Sun, T. & Morgan, H. Single-cell microfluidic impedance cytometry: a review. *Microfluidics and Nanofluidics* **8**, 423–443 (2010).
73. Guan, G. *et al.* Real-time control of a microfluidic channel for size-independent deformability cytometry. *Journal of Micromechanics and Microengineering* **22**, 105037 (2012).
74. Chuang, C.-H., Wei, C.-H., Hsu, Y.-M., Huang, H.-S. & Hsiao, F.-B. Impedance sensing of bladder cancer cells based on a single-cell-based DEP microchip. in 943–947 (2009). doi:10.1109/ICSENS.2009.5398183
75. Han, A., Yang, L. & Frazier, A. B. Quantification of the Heterogeneity in Breast Cancer Cell Lines Using Whole-Cell Impedance Spectroscopy. *Clinical Cancer Research* **13**, 139–143 (2007).
76. Schade-Kampmann, G., Huwiler, A., Hebeisen, M., Hessler, T. & Di Berardino, M. On-chip non-invasive and label-free cell discrimination by impedance spectroscopy. *Cell Prolif.* **41**, 830–840 (2008).
77. Küttel, C. *et al.* Label-free detection of Babesia bovis infected red blood cells using impedance spectroscopy on a microfabricated flow cytometer. *Acta Tropica* **102**, 63–68 (2007).
78. Malleo, D., Nevill, J. T., Lee, L. P. & Morgan, H. Continuous differential impedance spectroscopy of single cells. *Microfluidics and Nanofluidics* **9**, 191–198 (2009).
79. Holmes, D. *et al.* Leukocyte analysis and differentiation using high speed microfluidic single cell impedance cytometry. *Lab Chip* **9**, 2881–2889 (2009).
80. Morgan, H., Holmes, D. & Green, N. G. High speed simultaneous single particle impedance and fluorescence analysis on a chip. *Current Applied Physics* **6**, 367–370 (2006).
81. Mondal, D., Roychaudhuri, C., Das, L. & Chatterjee, J. Microtrap electrode devices for single cell trapping and impedance measurement. *Biomed Microdevices* **14**, 955–964 (2012).
82. Chen, J. *et al.* A microfluidic device for simultaneous electrical and mechanical measurements on single cells. *Biomicrofluidics* **5**, 014113–014113–11 (2011).
83. Guo, Q., Park, S. & Ma, H. Microfluidic micropipette aspiration for measuring the deformability of single cells. *Lab Chip* **12**, 2687–2695 (2012).
84. Hochmuth, R. M. Micropipette aspiration of living cells. *Journal of Biomechanics* **33**, 15–22 (2000).
85. Aingaran, M. *et al.* Host cell deformability is linked to transmission in the human malaria parasite Plasmodium falciparum. *Cell. Microbiol.* **14**, 983–993 (2012).
86. Guck, J. *et al.* Optical Deformability as an Inherent Cell Marker for Testing Malignant Transformation and Metastatic Competence. *Biophysical Journal* **88**, 3689–3698 (2005).
87. Chen, J. *et al.* Electrodeformation for single cell mechanical characterization. *J. Micromech. Microeng.* **21**, 054012 (2011).
88. MacQueen, L., Buschmann, M. & Wertheimer, M. Mechanical properties of mammalian cells in suspension measured by electro-deformation. *Journal of Micromechanics and Microengineering* **20**, 065007 (2010).
89. Voldman, J. ELECTRICAL FORCES FOR MICROSCALE CELL MANIPULATION. *Annual Review of Biomedical Engineering* **8**, 425–454 (2006).
90. MacQueen, L. A., Thibault, M., Buschmann, M. D. & Wertheimer, M. R. Electromechanical deformation of mammalian cells in suspension depends on their cortical actin thicknesses. *Journal of Biomechanics* **45**, 2797–2803 (2012).
91. Doh, I., Lee, W. C., Cho, Y.-H., Pisano, A. P. & Kuypers, F. A. Deformation measurement of individual cells in large populations using a single-cell microchamber array chip. *Applied Physics Letters* **100**, 173702–173702–3 (2012).

92. Lim, C. T. & Li, A. Mechanopathology of red blood cell diseases — Why mechanics matters. *Theoretical and Applied Mechanics Letters* **1**, 014000–014000–6 (2011).
93. Di Carlo, D., Aghdam, N. & Lee, L. P. Single-Cell Enzyme Concentrations, Kinetics, and Inhibition Analysis Using High-Density Hydrodynamic Cell Isolation Arrays. *Anal. Chem.* **78**, 4925–4930 (2006).
94. Gossett, D. R., Weaver, W. M., Ahmed, N. S. & Carlo, D. D. Sequential Array Cytometry: Multi-Parameter Imaging with a Single Fluorescent Channel. *Ann Biomed Eng* **39**, 1328–1334 (2011).
95. Taff, B. M. & Voldman, J. A Scalable Addressable Positive-Dielectrophoretic Cell-Sorting Array. *Anal. Chem.* **77**, 7976–7983 (2005).
96. Campbell, C. E., Laane, M. M., Haugarvoll, E. & Giaever, I. Monitoring viral-induced cell death using electric cell–substrate impedance sensing. *Biosensors and Bioelectronics* **23**, 536–542 (2007).
97. Cho, S., Becker, S., Von Briesen, H. & Thielecke, H. Impedance monitoring of herpes simplex virus-induced cytopathic effect in Vero cells. *Sensors and Actuators B: Chemical* **123**, 978–982 (2007).
98. Küllerich-Pedersen, K., Poulsen, C. R., Jain, T. & Rozlosnik, N. Polymer based biosensor for rapid electrochemical detection of virus infection of human cells. *Biosensors and Bioelectronics* **28**, 386–392 (2011).
99. McCoy, M. H. & Wang, E. Use of electric cell-substrate impedance sensing as a tool for quantifying cytopathic effect in influenza A virus infected MDCK cells in real-time. *Journal of Virological Methods* **130**, 157–161 (2005).
100. Dynamic and Label-Free Cell-Based Assays Using the Real-Time Cell Electronic Sensing System. *ASSAY and Drug Development Technologies* **4**, 597–607 (2006).
101. Archer, S., Morgan, H. & Rixon, F. J. Electrorotation Studies of Baby Hamster Kidney Fibroblasts Infected with Herpes Simplex Virus Type 1. *Biophysical Journal* **76**, 2833–2842 (1999).
102. Generalov, V. M. *et al.* Study of Virus–Cell Interaction by the Method of Dielectrophoresis. *Doklady Biochemistry and Biophysics* **383**, 82–84 (2002).
103. Perera, R. *et al.* Dengue Virus Infection Perturbs Lipid Homeostasis in Infected Mosquito Cells. *PLoS Pathogens* **8**, e1002584 (2012).
104. Mahoney, R. T. *et al.* Cost of production of live attenuated dengue vaccines: a case study of the Instituto Butantan, Sao Paulo, Brazil. *Vaccine* **30**, 4892–4896 (2012).
105. NIH & NIAID. Biodefense and Emerging Infectious Diseases. *NIAID Category A, B, and C Priority Pathogens* at <<http://www.niaid.nih.gov/topics/biodefenserelated/biodefense/pages/cata.aspx>>
106. Noisakran, S. *et al.* Cells in Dengue Virus Infection In Vivo. *Advances in Virology* **2010**, (2010).
107. Guo, J., Wang, W., Yu, D. & Wu, Y. Spinoculation Triggers Dynamic Actin and Cofilin Activity That Facilitates HIV-1 Infection of Transformed and Resting CD4 T Cells. *J. Virol.* **85**, 9824–9833 (2011).
108. Ye, L. *et al.* Centrifugal enhancement of hepatitis C virus infection of human hepatocytes. *Journal of Virological Methods* **148**, 161–165 (2008).
109. Schulze-Horsel, J., Genzel, Y. & Reichl, U. Flow cytometric monitoring of influenza A virus infection in MDCK cells during vaccine production. *BMC Biotechnol.* **8**, 45 (2008).
110. Hasnain, I. A. & Donald, A. M. Microrheological Characterisation of Anisotropic Materials. 3–7 (2008).
111. Mason, T. G., Ganesan, K., Van Zanten, J. H., Wirtz, D. & Kuo, S. C. Particle Tracking Microrheology of Complex Fluids. *Phys. Rev. Lett.* **79**, 3282–3285 (1997).
112. Fong, E. J. *et al.* Decoupling Directed and Passive Motion in Dynamic Systems: Particle Tracking Microrheology of Sputum. *Annals of Biomedical Engineering* **41**, 837 – 846 (2013).
113. Dow. Viscosity of Aqueous Glycerine Solutions. *OPTIM Synthetic Glycerine- Viscosity* at <<http://www.dow.com/safechem/optim/optim-advantage/physical-properties/viscosity.htm>>
114. Kurane, I., Kontny, U., Janus, J. & Ennis, F. A. Dengue-2 virus infection of human mononuclear cell lines and establishment of persistent infections. *Arch. Virol.* **110**, 91–101 (1990).

115. Heaton, N. S. *et al.* Dengue virus nonstructural protein 3 redistributes fatty acid synthase to sites of viral replication and increases cellular fatty acid synthesis. *Proc. Natl. Acad. Sci. U.S.A.* **107**, 17345–17350 (2010).
116. Epstein, M. A. *et al.* Morphological and Virological Investigations on Cultured Burkitt Tumor Lymphoblasts (Strain Raji). *JNCI J Natl Cancer Inst* **37**, 547–559 (1966).
117. Lambeth, C. R., White, L. J., Johnston, R. E. & Silva, A. M. de. Flow Cytometry-Based Assay for Titrating Dengue Virus. *J. Clin. Microbiol.* **43**, 3267–3272 (2005).
118. Teh, S.-Y., Khnouf, R., Fan, H. & Lee, A. P. Stable, biocompatible lipid vesicle generation by solvent extraction-based droplet microfluidics. *Biomicrofluidics* **5**, 044113–044113–12 (2011).
119. Khan, Z. S. & Vanapalli, S. A. Probing the mechanical properties of brain cancer cells using a microfluidic cell squeezer device. *Biomicrofluidics* **7**, 011806–011806–15 (2013).
120. Tan, S. J., Yobas, L., Lee, G. Y. H., Ong, C. N. & Lim, C. T. Microdevice for the isolation and enumeration of cancer cells from blood. *Biomed Microdevices* **11**, 883–892 (2009).
121. Hur, S. C., Henderson-MacLennan, N. K., McCabe, E. R. B. & Di Carlo, D. Deformability-based cell classification and enrichment using inertial microfluidics. *Lab Chip* **11**, 912–920 (2011).
122. Dewi, B. E., Takasaki, T. & Kurane, I. In vitro assessment of human endothelial cell permeability: effects of inflammatory cytokines and dengue virus infection. *Journal of Virological Methods* **121**, 171–180 (2004).
123. Peña, J. & Harris, E. Early Dengue Virus Protein Synthesis Induces Extensive Rearrangement of the Endoplasmic Reticulum Independent of the UPR and SREBP-2 Pathway. *PLoS ONE* **7**, e38202 (2012).

Timeline

Task		2012	2013	2014	2015
Aim 1	PTM develop de-trending algorithm	[Light blue bar spanning 2012, 2013, 2014, and 2015]			
	PTM simulations	[Light blue bar spanning 2012, 2013, 2014, and 2015]			
	PTM glycerol-water experiments	[Light blue bar spanning 2012, 2013, 2014, and 2015]			
	PTM sputum experiments	[Light blue bar spanning 2012, 2013, 2014, and 2015]			
Aim 2	Generation 1 device characterization	[Light blue bar spanning 2012, 2013, 2014, and 2015]			
	Generation 2 device characterization	[Light blue bar spanning 2012, 2013, 2014, and 2015]			
	Acoustic separation of cells and virus	[Light blue bar spanning 2012, 2013, 2014, and 2015]			
	Monitoring virus infection	[Light blue bar spanning 2012, 2013, 2014, and 2015]			
Aim 3	Electrode design, COMSOL simulations	[Light blue bar spanning 2012, 2013, 2014, and 2015]			
	Fabrication	[Light blue bar spanning 2012, 2013, 2014, and 2015]			
	Measurements	[Light blue bar spanning 2012, 2013, 2014, and 2015]			

Author's Vitae

Erika Fong
Lawrence Scholar
Lawrence Livermore National Laboratory
7000 East Ave, L-223, Livermore, CA 94550
Phone: 925-423-3596; Email: fong26@llnl.gov

(a) Professional Preparation

University of California, Los Angeles, CA	Computational and systems Biology	B.S. 2010
Boston University, Boston, Ma	Biomedical Engineering	PhD., estimated date of conferral 2016

(b) Appointments

2012- Present: Lawrence Scholar, MED, LLNL
Acoustic Filtering for Viral Biodetection and Evolution
UCOP Lab Fees Program, Team member
24 Month Diagnostic and Biosurveillance Challenge (DEPLOY)
DITRA, Team member

2010-Present: Graduate Researcher, Laboratory for Engineering Education and Development, Boston University

2009-2010: Undergraduate Researcher, DiCarlo Microfluidic Biotechnology Lab, UCLA

2008-2010: Peer Learning Facilitator, Academic Advancement Program, UCLA

June 2009- Sept 2009: Summer Student, SULI, Artificial Retina Project, LLNL

(c) Awards

2010: NSF Graduate Research Fellowship Program Honorable Mention

2011: Lawrence Scholar Fellowship, LLNL

(d) Publications

1. Fong, E.J., Johnston, A.C., Notton, T., Rose, K.A, Weinberger, L.S., Shusteff, M. Acoustic Focusing With Engineered Node Locations for High-Performance Microfluidic Ultrasonic Particle Separation. Manuscript under review.
2. Fong, E.J., Sharma, Y., Fallica, B., Tierney, D.B., Fortune, S.M., and Zaman, M.H. (2013). Decoupling Directed and Passive Motion in Dynamic Systems: Particle Tracking Microrheology of Sputum. *Annals of Biomedical Engineering* 41, 837 – 846.
3. Particle Tracking Microrheology in Non-Ideal Conditions for Characterization of Sputum Digestion. Annual meeting of the Biomedical Engineering Society (BMES), Atlanta, GA, October 24-27, 2012. Principal Presenter.